Czech Technical University in Prague
Faculty of Nuclear Sciences and Physical Engineering
Department of Physics

Programme: Applications of Natural Sciences
Branch of Study: Physics and Technology of Thermonuclear Fusion

Metal Hall sensors for measurement of magnetic field on fusion devices

Kovové Hallovy senzory pro měření magnetického pole na fúzních zařízeních

BACHELOR THESIS

Author: Milder Quispe Siles
Supervisor: Ing. Ivan Ďuran, Ph.D.
Submitted in: July 2016

Před svázáním místo téhle stránky vložíte zadání práce s podpisem děkana (bude to jediný oboustranný list ve Vaší práci) !!!!

Prohlášení

Prohlašuji, že jsem svou bakalářskou práci vypracoval samostatně a použil jsem pouze podklady uvedené v přiloženém seznamu. Nemám závažný důvod proti užití tohoto díla ve smyslu § 60 zákona č.121/200Sb. o právu autorském, o právech souvisejících s právem autorským a o změně některých zákonů (autorský zákon). V Praze dne ....

Milder Quispe Siles

Acknowledgement

First and foremost, I would like to express my gratitude to my thesis supervisor Ing. IvanĎuran, Ph.D. and thank him for his patience, guidance, support and advice during the timeof preparation of my bachelor thesis. Also, I would also like to thank Ing. Slavomír Enter forhelp and advice that he gave me during experiments. Without their assistance this paper wouldhave never been accomplished. Most importantly, none of this could have happened withoutmy family and girlfriend. Especially my mother, who offered her support despite the thousandkilometers that separate us.

Název práce:
Kovové Hallovy senzory pro měření magnetického pole na fúzních zařízeních
Autor: Milder Quispe Siles
Obor: Fyzika a technika termojaderné fúze
Druh práce: Bakalářská práce
Vedoucí práce: Ing. Ivan Ďuran, Ph.D.
Ústav fyziky plazmatu AVČR, v.v.i.

Abstrakt: Nejpouživatelnější metoda pro měření magnetického pole v tokamacích je založená na indukční cívce. Nicméně, i přes to, že tato metoda měří derivaci magnetického pole, integrování může být těžký úkol v některých případech. Kovové Hallové tensory jsou zajímavým alternativním řešením díky tomu, že dokážou měřit magnetické pole přímo. Především Hallové senzory založené na bismutu jsou perspektivní. Nicméně, takové jejich vlastnosti jako citlivost, linearita, atd. musí být dále studovány. Cílem teto bakalářské práce je popis a charakteristika těchto vlastností.
Klíčová slova: fuze, Hallonový sensor, magnetické pole, bismut, měření.

Title:
Metal Hall sensors for measurement of magnetic field on fusion devices
Author: Milder Quispe Siles

Abstract: The most used method for measurement of magnetic field in tokamaks is based on induction coils, this method measures the derivative of magnetic field and proper integration could be a difficult task in many cases. Metal Hall effect magnetic sensors are an attractive alternative solution due to the fact that they can directly measure the absolute value of magnetic field. Particularly Bismuth Hall based sensors show good perspective. However, its features such as sensitivity, linearity, etc. must be further studied. The objective of this bachelor thesis is the characterization of these properties.
Key words: fusion, Hall sensor, magnetic field, bismuth, measurement.

Contents

Contents 6

1 INTRODUCTION 8
1.1 Thermonuclear fusion 9
1.2 Drifts in plasma 12
1.3 Magnetic confinement devices 13

2 MAGNETIC DIAGNOSTICS 15
2.1 Induction methods 15
2.1.1 Mirnov Coils 15
2.1.2 Rogowski coils 17
2.2 Direct methods 18
2.2.1 Hall probes 18
2.2.2 Faraday rotation external to plasma 18

3 HALL EFFECTS SENSORS 20
3.1 The Classical Hall effect 20
3.1.1 Hall coefficient 21
3.1.2 Hall voltage 22
3.2 Generalization for a non-perpendicular magnetic field to current 23
3.3 Relevant galvanomagnetic effects to Hall effect 24
3.3.1 Planar Hall effect 24
3.3.2 Current deflection effect 24
3.3.3 Magnetoresistance 25
3.4 Main characteristics of Hall sensor 25
3.4.1 Sensor geometry 25
3.4.2 Sensitivity 26
3.4.3 Offset voltage 27
3.4.4 Linearity 27
3.5 DC and AC method 27
3.6 Requirements of Hall sensor for measurement of magnetic field on fusion devices 28
3.7 Metal based Hall sensors 29
3.7.1 Material selection 29
3.7.2 Design and construction technology 29
3.7.3 FISPACT activation analysis 30

4 EXPERIMENTAL EQUIPMENT 31

4.1 High-temperature coil . . . 31
4.2 Test bench . . . 34
4.3 Output signal processing . . . 35

5 RESULTS 37
5.1 Measured quantities . . . 37
5.2 Offset . . . 39
5.3 Sensitivity . . . 41
5.4 Linearity . . . 43
5.4.1 Hall voltage vs current . . . 43
5.4.2 Hall voltage vs magnetic field . . . 46
5.5 Amplification of the offset-cancellation electronics . . . 49

6 Summary and conclusions 50

Bibliography 52

Chapter 1

INTRODUCTION

Hall effect was discovered by the American physicist Edwin H. Hall (1885-1938) in 1879. He observed that when a current flows through a conductive plate placed in a magnetic field, a slight voltage appears in a direction perpendicular to both the current and to the magnetic field. This voltage was proportional to the current and magnetic field. The presence of this measurable transverse voltage is called Hall effect. Thanks to the fact that the voltage is proportional to the magnetic field, this effect becomes a useful tool for measuring magnetic fields.

The most common and successful method for measurement of magnetic field on fusion devices is based on magnetic induction coils. Using this method, it is possible to measure the variation in time of the magnetic field. Subsequently, using analog or numerical integration, it is possible to determine the absolute level of magnetic field. However, this method has some issues. If there are present relevant drifts, noise or pick-ups of other magnetic field component, the proper integration becomes a difficult task. For this reason, it is attractive to use a different method which could measure the absolute value of magnetic field itself and not its derivative.

It seems that the problem could easily be solved using a Hall effect sensor which can directly measure the absolute value of magnetic field. Nevertheless, there is a set of requirements such as high temperature resistance, high neutron fluence resistance, proper sensitivity, etc; that must be satisfied by the Hall sensor in order to be used on large fusion devices. This set of requirements does not allow application commercial Hall sensors that can be used. As a result, new Hall sensors are being developed.

Nowadays semiconductor based Hall sensors are very common in the industry of automobiles, computers, consumer devices, etc. These semiconductor based sensors have been extensively studied, firstly because of their low cost and secondly because of the high sensitivity compared to metals. Unfortunately for the fusion community, semiconductor based Hall sensors have limited applicability because, as mentioned above, the magnetic sensors are subjected to high temperatures. Moreover, the magnetic sensors are also subject to high neutron fluence in the case of large tokamaks such as the International Thermonuclear Experimental Reactor (ITER), which is been built next to the Cadarache (France); or the future Demonstration Power Station (DEMO). Despite these limitations, commercially produced Hall sensors Allegro where successfully applied for determination the position of the plasma in CASTOR[1] tokamak [28, 10] but without neutron fluence.

[1] In 2006, the tokamak CASTOR was transported to the Faculty of Nuclear Sciences and Physical Engineering of the Czech Technical University, where it serves under a new name GOLEM for education of students in the new curriculum Physics and Technology of the thermonuclear fusion[22].

Going a little further, investigations showed that the sensitivity change of InSb-based sensor (Specially produced by MSL Lviv), with optimal initial charge carrier concentrations under neutron fluence $F = 3 \times 10^{16}\, n \cdot cm^{-2}$ at temperature of $17^\circ\, C$; was equal to 0.8%[3]. Additionally, the sensitivity change at ITER relevant neutron fluences of $F = 10^{17} \div 10^{18}\, n \cdot cm^{-2}$ at temperature of $90^\circ C$ was equal to 7%. Subsequently, these sensors were successfully applied for the measuring of magnetic field pulses in the largest European thermonuclear reactors: TORE SUPRA, which is situated in Cadarache (France); and Joint European Torus (JET), which is situated in Culham (Great Britain)[4]. Hence, InSb-based sensor is a potential candidate for ITER ex-vessel steady state magnetic sensor.

Unlike semiconductor Hall based sensor, metal based ones are more compatible with high temperatures and radiation environment. Therefore, they have a good perspective to be part of the magnetic diagnosis in big fusion reactors. However, the investigation of the properties of metals, such as Hall sensors, started just few year ago. Therefore, it is necessary to characterize their properties, such as sensitivity, linearity, signal to noise ratio, etc. at big fusion devices environment. Particularly, at ITER ex-vessel SSMS environment. This bachelor thesis is focused on study of these properties for bismuth based Hall sensors.

1.1 Thermonuclear fusion

The nuclear fusion can be defined as a nuclear reaction between two light nuclei (atomic mass number $\boldsymbol{A}$ less than 56) that releases energy. When two nuclei come close to each other(collides), the Coulomb potential strongly repels them. However, if the distance between two nuclei becomes about $10^{-15}m$, the strong interaction becomes dominating and the nuclei fuse. As a result it is obtained a new nucleus with higher binding energy, new particles and a relatively large amount of energy.

In other words, two colliding nuclei with atomic number Z_a and Z_b, must overcome the maximal repulsion which is given at the distance of “contact” $R_0 = R_a + R_b$, where R_a and R_b are the equivalent radii of the two nuclei. The potential energy at R_0 is called *Coulomb barrier* and is given by

$$V(R_0) = \frac{e^2}{4\pi\varepsilon_0}\frac{Z_a Z_b}{R_0} \tag{1.1}$$

a useful approximation is $R_0 \approx R_p(Z_a^{1/3} + Z_b^{1/3})$ where $R_p = (1.3 - 1.7)\, fm$ is the proton radius.

The fusion process can be represented by

$$a + b \longrightarrow d + e + E_f, \tag{1.2}$$

where a and b are the original nuclei while d and e are the products. E_f represents the energy released by the process.

The Sun’s core can be considered as spherical plasma in thermodynamic equilibrium where the ions are primary hydrogen nuclei (protons). The energy source of the Sun is precisely a chain of nuclear reactions. The main chain of nuclear reactions in the Sun starts with simple protons and ends in He^4. It can be described by three steps[27]:

$$p + p \longrightarrow D + e^+ + \nu + \gamma + 9MeV \tag{1.3}$$

$$D + p \longrightarrow D + p \rightarrow He^3 + \gamma + 5.5MeV \tag{1.4}$$

$$He^3 + He^3 \longrightarrow He^4 + 2p + \gamma + 2.8MeV \tag{1.5}$$

The number density and temperature in the Sun's core are around $n \approx 6 \times 10^{25}\, 1/cm^3$ and $T \approx 1.57 \times 10^7\, K$ respectively[19]. Considering the Sun's core plasma in thermodynamic equilibrium and in the absence of any field force effect, its particles of mass m moving in a sufficiently large volume follow the Maxwell-Boltzmann energy distribution function. Under this conditions, the probability that two protons could approach within 1 fm would be $\sim 10^{-152}$ if classical physics applied. However, they do with a probability $\sim e^{-16}$. It is possible due quantum mechanical tunneling.

When the nuclei are single protons ($p-p$ *reaction*) the strong interaction do not keep them together, the diproton ^2He is very unstable and it has a negligible half-life. Therefore, only when a proton decays into a neutron through weak interaction (during the brief time that the two protons approach within 1 fm), the strong interaction keeps them together, resulting in deuterium, new particles and energy but the probability of this events will be$\sim 10^{-30}$. This is an unfortunate result for practical applications, but it is the reason of the stability of the Sun.

Analyzing the situation of the Sun's core, a large amount of plasma(formed by protons and electrons) is confined by gravity; under this conditions fusion take place. However, the situation on Earth is much different. On the one hand, it is not possible to use hydrogen as a fuel because, as mentioned above, a proton must decay into a neutron through weak interaction and the probability of this event is very small. Additionally, it is not possible to use the gravity to confine the plasma on Earth. These problems can be solved:

1. Using a fuel which does not depend on weak interaction, e.g. a mixture of deuterium and tritium.

2. Confining the plasma using magnetic devices as tokamaks or stellerators (magnetic confinement fusion) or compressing a small fuel pellet by an intense pulse of energy (Inertial confinement fusion).

For practical applications it is needed to know the *fusion power density* S_f, which determines the power per unit volume in a fusion reactor core. S_f is evidently governed by the *fusion reaction rate* R_{ab}, which determines the number of fusion collision per unit volume per unit time. Once the value of R_{ab} is known, then it is easy to calculate the fusion power produced per unit volume

$$S_f = E_f R_{ab} \qquad [W/m^3]. \tag{1.6}$$

In general, to describe the fusion reaction rate R_{ab} of any plasma, the proportionality factor σ expressed in m^2 is used, that involves the effects of strong interaction, weak interaction, etc. This factor is called cross section and it is intimately connected with the occurrence of a reaction.

For the simple case of two intersecting beams of mono-energetic particles, as is shown in figure 1.1, it is possible to derive an expression for the fusion reaction rate

$$R_{ab} = n_a n_b \sigma v \qquad [1/m^3 s] \tag{1.7}$$

where n_a and n_b are the number density (expressed in number of particles per unit volume) of particles of type a and type b, respectively; v is the relative sped of the two set of particles at the point of intersection; and σ is the proportionality factor(cross section). It is possible to calculate an approximation for cross section using quantum mechanics, but for fusions reactions cross sections are determined experimentally. Cross section is a universal parameter, which only depends on energy, type of colliding particles and kind of interaction.

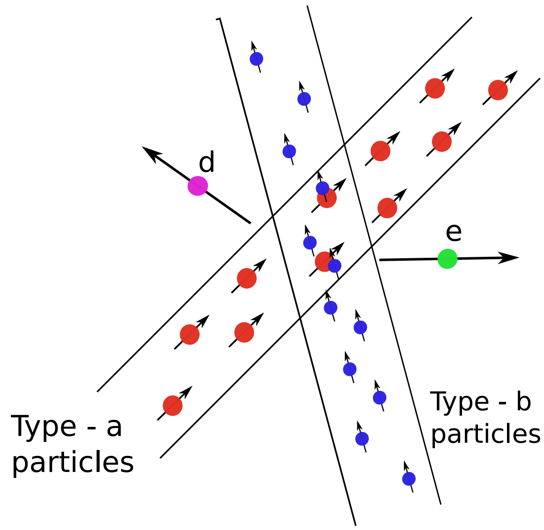

Figure 1.1: Intersection of two particle beams resulting in fusion reaction $a + b \to d + e$

The equation (1.7) describes just the case when all particles possess a constant speed, and their motion is mono directional. However, the particles have a range of speeds and are moving in various directions in a real plasma. Therefore equation (1.7) must be generalized in order to include a summation over all particle energy and all direction of motion. For this purpose it is used the distribution function $f(\vec{r}, \vec{v}, t)$; the densities n_a and n_b must be replaced by $n_a \to n_a f_a(v_a) d\vec{v}_a$ and $n_b \to n_b f_b(\vec{v}_b) d\vec{v}_b$, respectively; the relative velocity must be $v = |\vec{v}_a - \vec{v}_b|$; and finally the cross section must be a function of relative speed $\sigma = \sigma\left(|\vec{v}_a - \vec{v}_b|\right)$. Combining these modifications leads

$$R_{ab} = n_a n_b \left\langle \sigma v \right\rangle_{ab} \tag{1.8}$$

where was introduced the *reactivity* $\left\langle \sigma v \right\rangle_{ab}$ given by

$$\left\langle \sigma v \right\rangle_{ab} = \int f_a(\vec{v}_a) f_b(\vec{v}_b) \sigma\left(|\vec{v}_a - \vec{v}_b|\right) |\vec{v}_a - \vec{v}_b| \, d\vec{v}_a d\vec{v}_b \tag{1.9}$$

Replacing (1.8) into (1.6) we obtain an expression for the *fusion power density* in plasmas

$$S_{ab} = E_f n_a n_b \left\langle \sigma v \right\rangle_{ab} \tag{1.10}$$

The main fusion reactions of interest are:

$$D + T \longrightarrow \alpha(3.52\ Mev) + n(14.06\ Mev) \tag{1.11}$$
$$D + D \longrightarrow T(1.01\ Mev) + p(3.03\ Mev) \tag{1.12}$$
$$D + D \longrightarrow {}^3He(0.82\ Mev) + n(2.45\ Mev) \tag{1.13}$$
$$D +^3 He \longrightarrow {}^4He(3.67\ Mev) + p(14.67\ Mev) \tag{1.14}$$

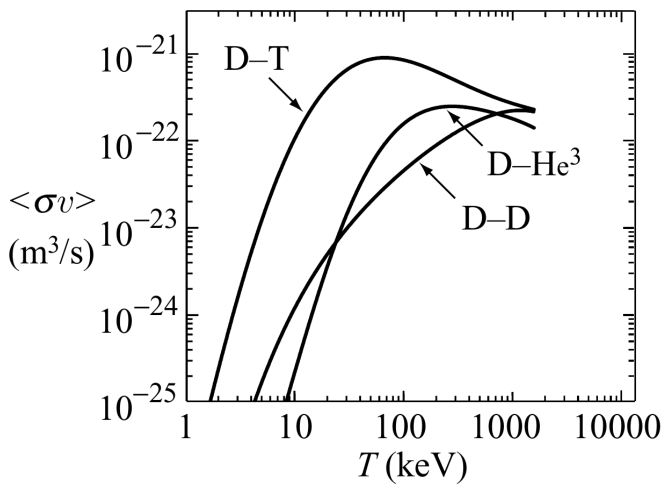

Figure 1.2: Reactivity for $D-T$, $D-He^3$ and $D-D$ fusion reactions in a Maxwellian-distributed plasma as a function of temperature [14].

The figure 1.2 illustrates the reactivity for the main fusion reactions of interest. It shows that in terms of reactivity D-T is the best option. However, there is one problem: the half-live of tritium is approximately 12.31 years. Therefore, there is no tritium in the nature. Fortunately tritium can be produced within the fusion reactor: if we place a lithium blanket around the plasma, the neutrons (which carry approximately the 80% of total released energy), that leave the plasma, can interact with lithium and produce tritium according to the following relation:

$$n +^6 Li \longrightarrow \alpha(2.2\ Mev) + T(2.7\ Mev) \tag{1.15}$$

In order to obtain a fully ionized plasma and achieve the conditions for fusion, the D-T fuel must be heated by an external source to temperatures in the range of tens of keV. The moment, when the production of alpha particles by D-T reaction is enough to maintain the plasma hot without using external sources (the reactor is self-sufficient), is called *ignition*. The conditions to achieve ignition are given by the Lawson criterion [35]:

$$n\tau_E T > 30 \cdot 10^{20} keV s/m^3 \tag{1.16}$$

where $n = n_D + n_T$, τ_E is the energy confined time and T is the temperature in the range of $10 \div 20\ keV$.

1.2 Drifts in plasma

In presence of a magnetic field, the plasma particles move along the magnetic field lines with a gyro motion around so called guiding center. The radius of this gyro motion is called *Larmor radius* $r_L = \frac{mv_\perp}{|q|B}$, where $v_\perp$is speed of particle in plane perpendicular to $\vec{B}$, q is the charge of particle and m is the mass of particle. The gyro motion has a frequency called *cyclotron frequency* $\omega_c = \frac{|q|B}{m}$.

When a force accelerates a particle, the velocity increases and higher velocity means a larger Larmor radius. Therefore, the circular orbit no longer closes on itself resulting in a drift. In general, it is possible to write the motion of a particle as a sum of the motion along the magnetic field $\hat{e}_B v_\parallel$, the gyro motion $\vec{v}_{gyr}$ and the total drift $\vec{v}_{drift}$

$$\vec{v} = \hat{e}_B v_{\parallel} + \vec{v}_{drift} \tag{1.17}$$

The concrete form of $\vec{v}_{drift}$ depend on the external force(if there is one) and on the nature of $\vec{E}$ and $\vec{B}$. Table 1.1 summarize the different drifts.

Kind of drift	symbol	Expression
General force drift	$\vec{v}_F$	$\frac{1}{q}\frac{\vec{F}\times\vec{B}}{B^2}$
$E \times B$ drift	$\vec{v}_{E\times B}$	$\frac{\vec{E}\times\vec{B}}{B^2}$
Polarization drift	$\vec{v}_p$	$\frac{m}{qB^2}\frac{d\vec{E}_\perp}{dt}$
Grad-B drift	$\vec{v}_{\nabla B}$	$\frac{mv_\perp^2}{2qB}\frac{\vec{B}\times\nabla\vec{B}}{B^2}$
Curvature drift	$\vec{v}_R$	$\frac{mv_\parallel^2}{qB}\frac{\vec{B}\times\nabla\vec{B}}{B^2}$

Table 1.1: Different drifts in plasma[5]. The symbols $\parallel$ and $\perp$ refer to the component of the vector parallel and perpendicular to magnetic field.

1.3 Magnetic confinement devices

It is possible to confine the plasma (in radial direction) using so called θ-pich. This is a set of coils placed in a imaginary cylinder that generates a relative homogeneous magnetic field along the cylinder axis, thus plasma is confine in radial direction, but charged particles can move freely along the axis of the cylinder, therefore a torus is used in stead of cylinder to close the ends. It seams the problem is solved; nevertheless, the magnetic field is no longer homogeneous in this new configuration, as drifts are present.

It is not difficult to prove that the magnetic field in toroidal direction is given by $\vec{B}_\phi = B_t\hat{e}_\phi$, where $B_t = R_0 B_{t0}/R$, that means that there is a gradient of B in radial direction. This dependence is illustrated in Fig.1.3a. Using the definition of grad-B drift from table 1.1 it is obtained $\vec{v}_{\nabla B} = \frac{\mu}{qR}\hat{e}_z$, which means that ions drift up and electrons drift down(see Fig.3.1b) resulting in an electric field $\vec{E} = -E\hat{e_z}$. Again, using the definition of $E \times B$ drift from table 1.1 it is obtained $\vec{v}_{E\times B} = \frac{E}{B_t}\hat{e}_r$, which means that ions as well as electrons will drift out from the plasma in radial direction. The solution to this outward drift is the creation of a poloidal magnetic field $\vec{B}_\theta$ that short-circuits the charge accumulation. This can be done by:

- driving a current through the plasma using the transformer principle.
- breaking the axial symmetry.

The device with a poloidal magnetic field generated by driving a current through plasma, described above, is called *Tokamak*. Its basic components are illustrated in Fig. 1.4

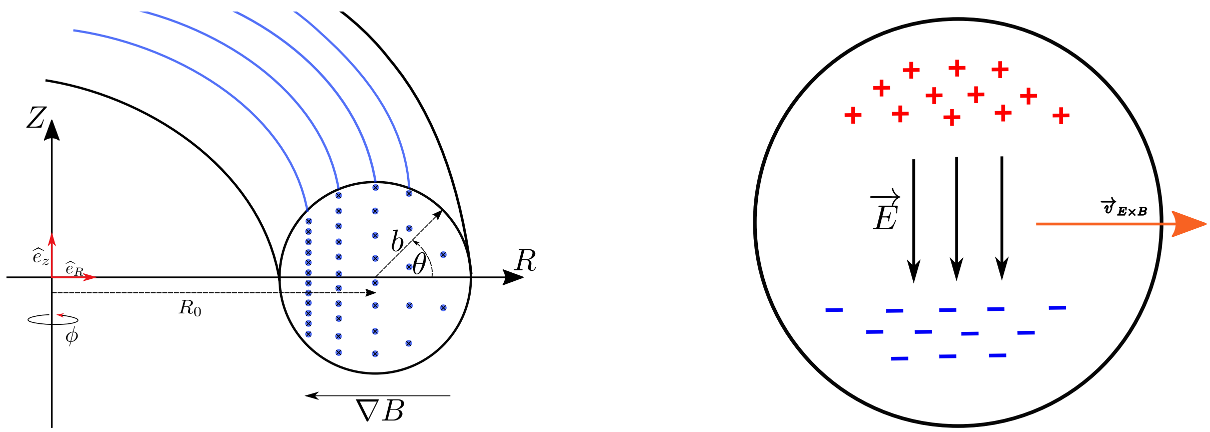

(a) (b)

Figure 1.3: (a) Schematic view of torus with θ-pinch. (b) Present drifts

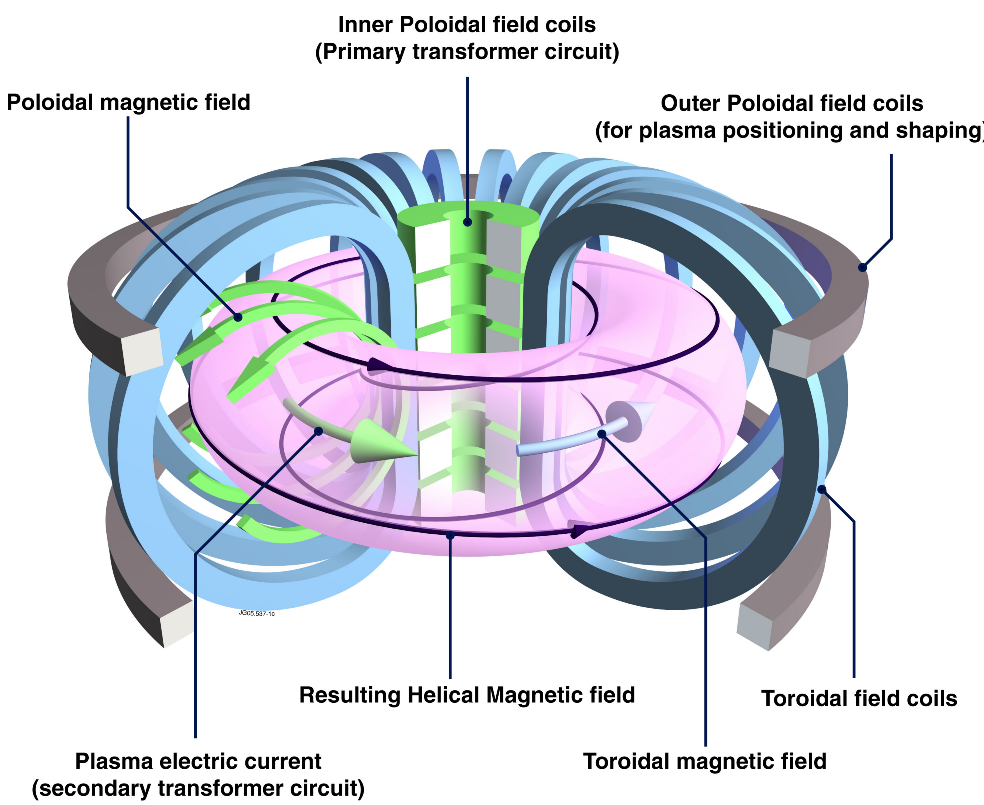

Figure 1.4: Basic components of tokamak[13]

Chapter 2

MAGNETIC DIAGNOSTICS

Magnetic diagnosis is the general name for different type of measurement of the magnetic field inside and outside the plasma. Thanks to the fact that a time-varying magnetic field induces an electric field, it is possible to use coils to determine magnetic field (*induction methods*), this methods are the most used in tokamaks due to their simplicity and relative low cost. Different coil configurations (such as Mirnov coils or Rogowski coils) allow measuring the time variation of magnetic field inside and outside of plasma, then it is necessary to integrate it to obtain the absolute level of magnetic field. It can be done numerically or analogically. However, if the magnetic field remains constant over the time, there is no signal to integrate. Additionally, the radiation in tokamaks induces some undesirable effect in inductive sensors, namely: the radiation induced electromotive force (RIEMF)[34], radiation induced conductivity (RIC)[30], radiation induced electric degradation (RIED)[30].

The are other alternative methods, which can measured magnetic field directly, such as fiber optic based on Faraday effect or Hall effect sensors (*direct methods*).

2.1 Induction methods

2.1.1 Mirnov Coils

A Mirnov coil is a simple small wire coil based on the Faraday's law, figure 2.1 illustrates its configuration with an integration circuit. If a magnetic field is varying over the time, the Mirnov coil provides a voltage proportional to the rate of change of magnetic field B. Solving the integral form of the Faraday's law, this voltage is given by

$$V = NA\dot{B} \tag{2.1}$$

where N is the number of turns in the coil and A is the area of the coil.

Integration

As mentioned above, equation 2.1 must be integrated in order find the absolute level of magnetic field. Fig.2.2 show two typical circuit (passive and active), which can be used for this purpose. Solving the passive-integration circuit, the integrated signal V_{out} will be given by

$$V_{out} = \frac{1}{1 + i\omega RC} V_{in} \approx \frac{1}{RC} \int V_{in} dt \quad (\omega RC \gg 1) \tag{2.2}$$

consequently, the absolute value of the magnetic field will be given by

$$B = \frac{RC}{AN} V_{out} \tag{2.3}$$

Equation 2.2 is limited by the condition $\omega RC \gg 1$, whereas increasing RC decreases the amplitude of output voltage, the passive integration circuit can be used just for high frequency bandwidth. An improved alternative method is the active-integration circuit(see Fig. 2.2b). In this case, the output voltage V_{out} is given by

$$V_{out} = -\frac{G}{1 + i\omega RC + iG\omega RC} V_{in} \approx -\frac{1}{RC} \int V_{in} dt \quad (G\omega RC \gg 1) \tag{2.4}$$

where G is gain of operational amplifier, this method allows as to measure magnetic fields even in timescales $1 \div 10$ s[32]. However, if relevant drifts, noise or pick-ups of other magnetic field component in V_{in} are present, they will be integrated as well. In this case, the output voltage V_{out} could not be reliable. So it is the biggest disadvantage of induction methods.

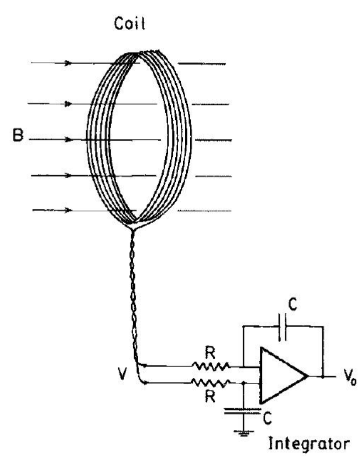

Figure 2.1: Schematic drawing of typical Mirnov coil and integration circuit[17]

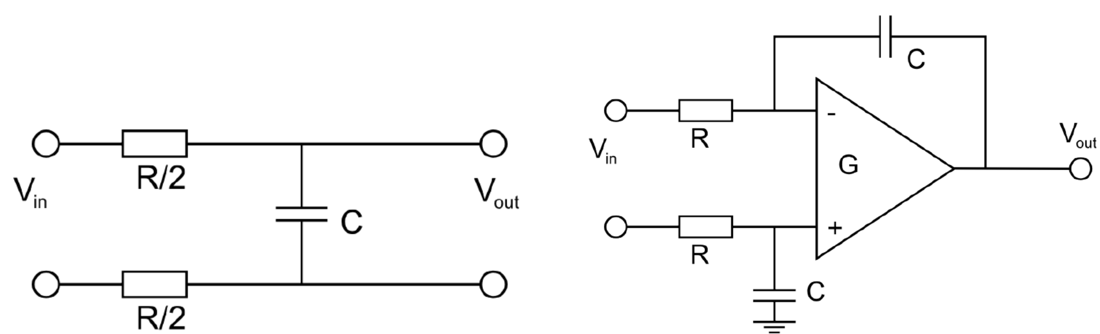

(a) (b)

Figure 2.2: Typical integrative circuit for the coil signal: passive (a), active (b) [32]. V_{in} - voltage provided by the Mirnov coil, V_{out} - integrated signal.

Plasma position

The distribution of plasma density is determined by the distribution of plasma magnetic surfaces. Therefore, a measurement of the poloidal magnetic field would give information about the position of the plasma column in tokamaks. Mirnov coils are the most used for this purpose magnetic sensors. A set of small Mirnov coils are placed around the plasma column as illustrated in figure 2.3. If the plasma column is centered, then all Mirnov coils should measure the same signal whereas the plasma column is displaced upwards, then the upper Mirnov coils should measure an increased signal.

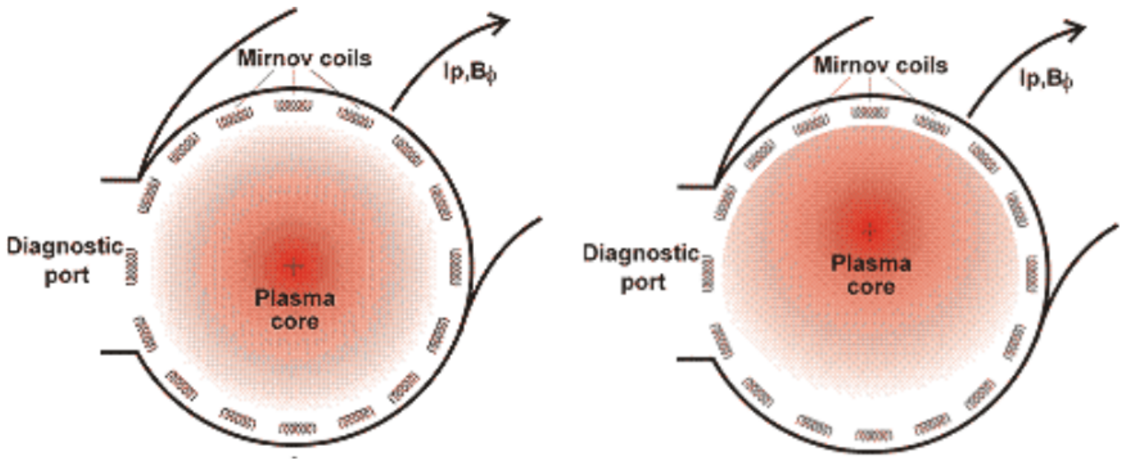

Figure 2.3: Plasma position on tokamak [29]

2.1.2 Rogowski coils

The Rogowski coil is a variation of the Mirnov coil where the ends are brough around together forming a torus as can be seen in figure 2.4a. Note that the ends are not closed, instead, the wire comes back along the axis of the solenoid. This is done in order to increase the accuracy[26]. This device is based on Ampes's law and can measure high frequency current (thus the poloidal magnetic field generated by the current). Similarly to Mirnov coil, using the integral form of Ampes's law, it is possible to derive an expression for induced voltage generated by the current

$$V_{coil} = -\mu_0 N A \dot{I} = -M \dot{I} \tag{2.5}$$

where μ_0 is the air permeability, N is the number of turns per unit length and A is the turn area.

The Rogowski coil is equivalent to the RCL circuit shown in Figure 2.5[1]. If a measurable impedance is placed in the coil's ends, then the relation between the induced voltage V_{coil} and the measured voltage V_{out} is given by

$$\frac{V_{out}}{V_{coil}} = \frac{Z}{L_c Z C_c j^2 \omega^2 + (L_c + R_c Z C_c) j\omega + R_c + Z} \tag{2.6}$$

where R_c is the coil resistance, L_c is the coil inductance, C is the coil capacitance, j is the current density and ω is the frequency of the circuit.

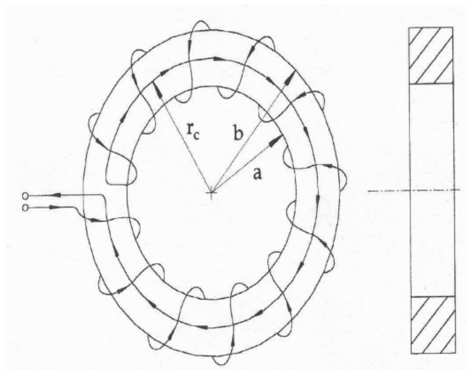

(a) [26]

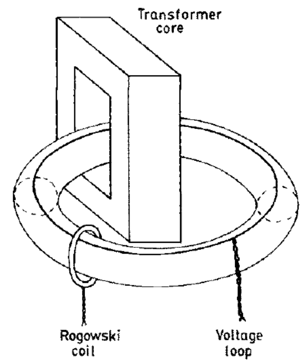

(b)

Figure 2.4: Rogowski coil: single-layer Rogowski coil with a counter-woun compensation turn (a), Rogowski coil in tokamaks (b)

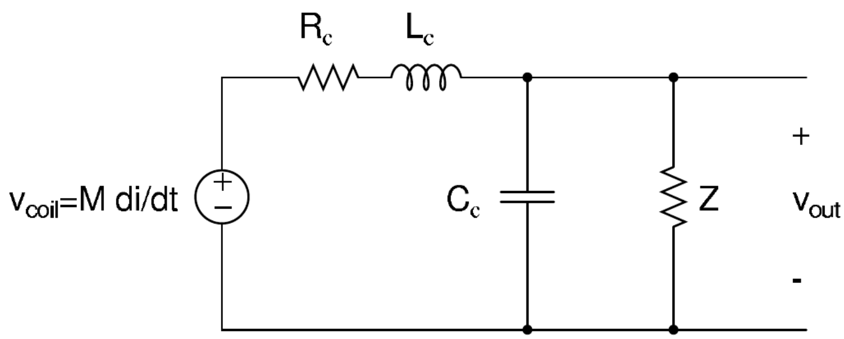

Figure 2.5: RCL circuit equivalent to Rogowski coil, R_c - coil resistance, L_c - coil inductance, C - coil capacitance[1]

2.2 Direct methods

2.2.1 Hall probes

The Hall probes are based on principle of the Hall effect. It is the the main topic of this bachelor thesis and we have dedicated a whole chapter for this. (see chapter 3).

2.2.2 Faraday rotation external to plasma

When a polarized light passes through a medium subjected to a magnetic field, the plane of polarization of the light rotates, see Fig.2.6. This is called Faraday effect. It has been used in fusion devices to measure both internal and external magnetic fields to plasma. Similarly to Rogowski coil, an optic fiber encompasses the torus outside of plasma and it is used a laser beam. The magnetic field generated by the plasma current, induces a birefringence in the fiber optic, producing a Faraday rotation of the polarization of the light in the optic fiber. The Faraday rotation ψ is proportional to the current I [23], then

$$\psi = \mu V \cdot I \tag{2.7}$$

where μV is the *Verdet constant*. For a infrared light ($\lambda = 1500\ nm$) the Verdet constant is $\mu V = 0.7\ \mu rad/A$.

As well as Hall sensors this method directly measures the absolute value of magnetic field. The disadvantage of this method is that radiation can damage the fiber and temperature changes can affect the linearity.

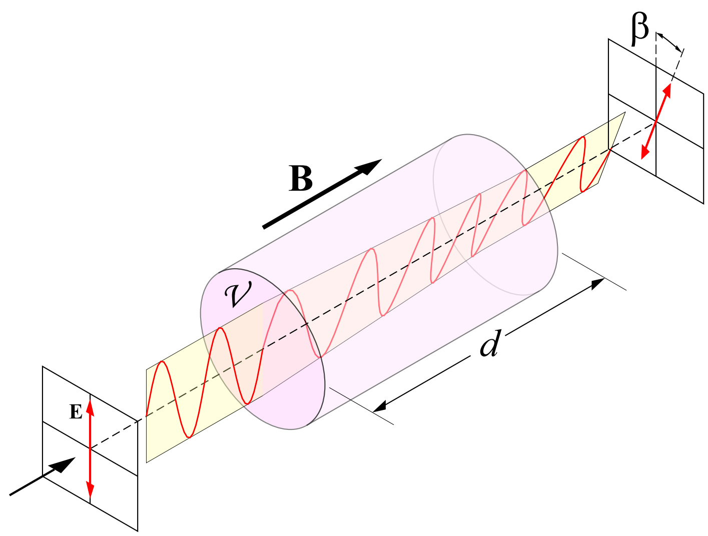

Figure 2.6: Polarization rotation due to the Faraday effect[36]

Chapter 3

HALL EFFECTS SENSORS

All electrical or thermal phenomena observed in a conductive material which is placed perpendicular to a magnetic field, are called *galvanomagnetic effects*. Hall effect is one of them. It was discovered by American physicist Edwin H. Hall(1885-1938) in 1879. He observed that when a current flows through a conductive plate placed in magnetic field, a slight voltage appears in direction perpendicular to both current and magnetic field. This voltage was proportional to current and magnetic field. The presence of this measurable transverse voltage is called Hall effect. Thanks to the fact, that voltage is proportional to magnetic field, this effect becomes a useful tool for measuring magnetic fields.

3.1 The Classical Hall effect

All galvanomagnetic effects are caused by free charge transport of carrier as a consequence of action of the Lorentz force on them. If free charge carriers are electrons, then the Lorentz force acting on them is given by

$$\vec{F} = -e\vec{E}_e - e[\vec{v} \times \vec{B}] \tag{3.1}$$

where e denotes the elementary charge $1.6022 \cdot 10^{-19}\ C$, $\vec{E}_e$ is external electric field, $\vec{v}$ denotes the electron velocity and $\vec{B}$ is the magnetic field.

In the following analysis we will neglect the thermal motion of carriers in order to simplify the calculations. Thus, the result we will obtain will be an approximation.

Let us consider a thin plate of conductive material, such as copper as it is shown in Fig. 3.1a. Assuming that the length l of the plate is much larger than its width w (in order to neglect the influence of the contacts in the plate), when a potential difference is applied to their ends an external electric field $\vec{E}_e = E_x\hat{e}_x$ is generated along the length of the plate as is shown in Fig. 3.1a. The electrons which have normally random velocities in all directions, drift in opposite direction to $\vec{E}_e$. The drift velocity is given by

$$\vec{v}_d = -\mu\vec{E}_e \tag{3.2}$$

where μ is the *electron mobility*[24]. There is a drift current density $\vec{J}$ associated with this drift velocity given by

$$\vec{J} = -en\vec{v}_d = \mu en\vec{E}_e \tag{3.3}$$

where n, is *free electron density*[1] of the plate's material. The proportionality coefficient $\sigma = \mu en$ is called *electric conductivity*, and its inverse $\rho = \frac{1}{e\mu n}$ is called *electric resistivity*. Then Eq. (3.3) can be written as

$$\vec{J} = \sigma \vec{E}_e. \tag{3.4}$$

It is possible to find the total current passing through plate form (3.3)

$$\begin{aligned} I &= \int_S \vec{J} \cdot d\vec{S} \\ &= J \int d\vec{S} \\ &= \mu en E_x wd \end{aligned} \tag{3.5}$$

If a magnetic field is applied to plate in direction $\hat{e}_y$, i.e. $\vec{B} = B_y \hat{e}_y$ as shown in Fig. 3.1b, the electrons moving through the plate are pushed in direction $\hat{e}_z$ by the magnetic force $\vec{F}_m = -e\vec{v}_d \times \vec{B} = ev_d B_y \hat{e}_z$. Therefore, there is a negative(electrons) and positive(holes) charge accumulation on the top and on the bottom of the plate, respectively. As a result, an electric field appears in direction $\hat{e}_z$. This field is called *Hall electric field* $\vec{E}_H = E_H \hat{e}_z$. Consequently, an electric force is establish in opposite direction to magnetic force, i.e. $\vec{F}_H = -eE_H \hat{e}_z$. The electron displacement in direction $\hat{e}_z$ is stopped at the moment, when the Hall electric force is big enough to balance the magnetic force.

$$-e\vec{E}_H - e[\vec{v}_d \times \vec{B}] = 0 \tag{3.6}$$

From this moment on, the electrons again start to move in direction $-\hat{e}_x$, as if only the external electric field $\vec{E}_e$ was acting.
Using Eq. (3.2) and (3.6) the Hall electric field is

$$\vec{E}_H = \mu[\vec{E}_e \times \vec{B}] \tag{3.7}$$

and in our particular case

$$\vec{E}_H = \mu E_x B_y \hat{e}_z. \tag{3.8}$$

3.1.1 Hall coefficient

Combining Eq. (3.3) and (3.7) it is possible to write the Hall field in terms of current density and magnetic field

$$\vec{E}_H = -R_H[\vec{J} \times \vec{B}]. \tag{3.9}$$

where a parameter called *Hall coefficient* R_H was introduced

$$R_H = -\frac{1}{en} \tag{3.10}$$

[1]The general term referring to electrons and holes is *carrier density*. In the case of semiconductors, carrier density is usually referred as *carrier concentration*.

3.1.2 Hall voltage

Associated with the Hall electric field, there is a voltage called Hall voltage V_H, this voltage is a more tangible quantity, which can be measured directly. It is generally given by

$$V_H = \int_a^b \vec{E}_H \cdot d\vec{z}$$

in our particular case using 3.8

$$V_H = -\int_0^w E_H dz = E_H w = -\mu E_x B_y w \tag{3.11}$$

For practical applications it is useful to express the Hall voltage V_H in terms of macroscopic and integrals quantities . Then replacing E_x from (3.5) into relation bellow, we finally obtain

$$V_H = -\frac{1}{en}\frac{IB_y}{d} = \frac{R_H}{d} I_H B_y \tag{3.12}$$

where a subscript H in the current was introduced to specify that this current is passing through the Hall sensor. Equation (3.12) tell as that the Hall voltage is inversely proportional to free charge carrier of the material, that is why the semiconductor based Hall sensors provides bigger Hall voltage than metal based ones. The amount of output signal (Hall voltage) provided by the Hall sensor is charachterizied by its *sensitivity*(see section 3.4.2)

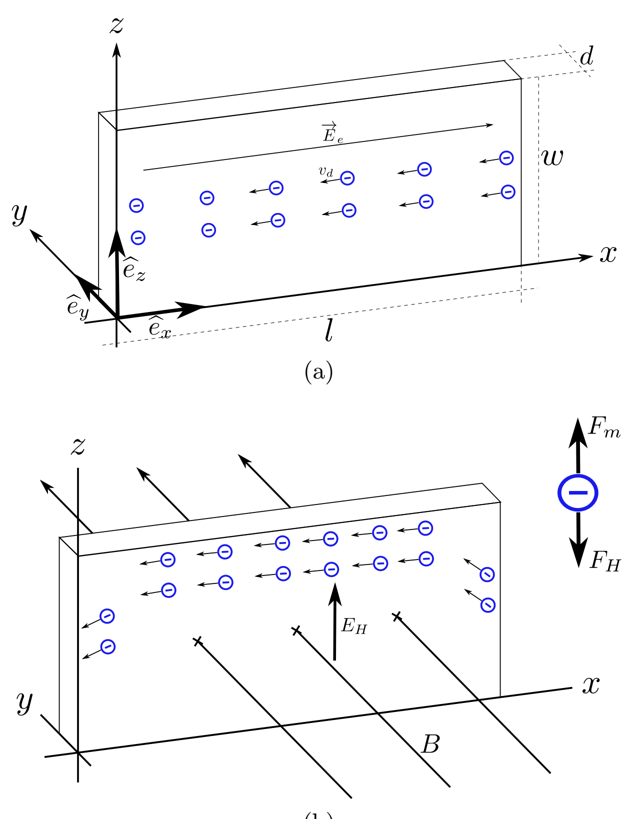

Figure 3.1: Hall effect in a conductive plate

3.2 Generalization for a non-perpendicular magnetic field to current

The analysis we did until now was assuming that the magnetic field was always perpendicular the electric field and the length of plate was much bigger than its width. If we take the general case in which we only assume that $\vec{E}$ and $\vec{B}$ are known, the general solution can be obtained by solving the equation (3.1).

With the purpose of finding a solution for $\vec{J}$, we will rewrite the equation 3.1 in terms of $\vec{J}$. It can be done by replacing Lorentz force $\vec{F}$ by the equivalent electrical force $-e\vec{E}$ and subsequently multiplying the result by $-\mu n$:

$$-e\vec{E} = -e\vec{E}_e - e[\vec{v} \times \vec{B}] \tag{3.13}$$

$$\vec{J}(\vec{E}) = \sigma\vec{E} - \mu[\vec{J}(\vec{E}) \times \vec{B}] \tag{3.14}$$

Solving this vectorial equation for $\vec{J}(\vec{E})$ we obtain

$$\vec{J}(\vec{E}) = \sigma_B\vec{E} - \mu\sigma_B[\vec{E} \times \vec{B}] + \mu^2\sigma_B(\vec{E} \cdot \vec{B})\vec{B} \tag{3.15}$$

$$\vec{J} = \vec{J}_1 + \vec{J}_2 + \vec{J}_3 \tag{3.16}$$

where

$$\sigma_B = \frac{\sigma}{1 + \mu^2 B^2}$$

This result tells us that total current density is a combination of three different components, $\vec{J}_1$ is proportional to $\vec{E}$; $\vec{J}_2$ is perpendicular to $\vec{E}$ and it is responsible of the Hall effect; $\vec{J}_3$ (which vanishes when the magnetic field is perpendicular to electric field) is proportional to $\vec{B}$ and it is the responsible of the so called *planar Hall effect*.

The solution $\vec{J}(\vec{E})$ from (3.15) can be alternatively expressed for its inverse $\vec{E}(\vec{J})$

$$\vec{E}(\vec{J}) = \rho_B\vec{J} + \mu\rho_B[\vec{J} \times \vec{B}] + \mu^2\rho_B(\vec{J} \cdot \vec{B})\vec{B} \tag{3.17}$$

$$\vec{E} = \vec{E}_1 + \vec{E}_2 + \vec{E}_3 \tag{3.18}$$

where

$$\rho_B = \frac{\rho}{1 + \mu^2 B^2} \tag{3.19}$$

An accurate analysis, which involves thermal motion of carriers can be found in [24]. This accurate treatment, which is based on the solution of Boltzmann kinetic equation changes Eq. (3.15) and (3.17) just in the coefficients as follows:

$$\vec{J}(\vec{B}) = \tilde{\sigma}_B\vec{E} - \mu_H\tilde{\sigma}_B[\vec{E} \times \vec{B}] + Q_H(\vec{E} \cdot \vec{B})\vec{B} \tag{3.20}$$

$$\vec{E}(\vec{J}) = \rho_b\vec{J} + \tilde{R}_H[\vec{J} \times \vec{B}] + P_H(\vec{J} \cdot \vec{B})\vec{B} \tag{3.21}$$

where $\tilde{\sigma}_B$ is the *Corbino conductivity*, μ_H is the *Hall mobility*, Q_H is the *planar Hall-current coefficient*, ρ_b is the *intrinsic magnetoresistivity*, $\tilde{R}_H$ is the *generalized Hall coefficient* and P_H is the *planar Hall coefficient[24].*

The Hall mobility μ_H and generalized Hall coefficient $\tilde{R}_H$ are related with the electron mobility μ and Hall coefficient R_H (3.10) as follows:

$$\mu_H = r_H \mu \tag{3.22}$$
$$\tilde{R} = r_H R_H \tag{3.23}$$

where r_H is the Hall *scattering factor.* This numerical factor in most cases differs from unity by less than 20%[29], therefore (3.9) is a good approximation.

3.3 Relevant galvanomagnetic effects to Hall effect

3.3.1 Planar Hall effect

As we have mentioned above, a magnetic field perpendicular to direction of the current in a plate induces a voltage perpendicular to both current and magnetic field. However, if magnetic field is no longer perpendicular to the current, the perpendicular component of this new magnetic field to the current will continue generating a voltage, while the parallel component to the current will additionally induce an electric field in direction of magnetic field and consequently an additional voltage. The presence of this new voltage is called *planar Hall effect* and it was first observed by Goldberg and Davis in 1954. It can be clearly seen analyzing equation (3.21). The third term of the total electric field is

$$E_B = P_H(\vec{J} \cdot \vec{B})\vec{B} \tag{3.24}$$

this is called *planar Hall electric field* and appears when the magnetic field is not perpendicular to the current. Otherwise, E_B vanishes and we have only Hall effect.

In general the total output voltage is given by

$$V_{out} = V_H + V_P \tag{3.25}$$

3.3.2 Current deflection effect

Let us consider the same plate from figure (3.1a), but with the particularity that $l \ll w$. In this case, there will not be a Hall voltage. Instead, there will be a transverse current in the plate.

Equation (3.14) can be rewritten in terms of current density:

$$\vec{J}(\vec{B}) = \vec{J}(0) - \mu[\vec{J}(\vec{B}) \times \vec{B}] \tag{3.26}$$

where $\vec{J}(\vec{B}) = -e\mu v$ is the electron current density in presence of a magnetic field, and $\vec{J}(0) = e\mu n\vec{E}$ is the drift current density due to the external electric field when $\vec{B} = 0$. The equation (3.26) is graphically represented in figure 3.2. As we can see the current density $\vec{J}(0)$ due to the external electric field and the current density in presence of the magnetic field $\vec{J}(B)$ are not collinear. In other words, if conductive plate is short($l \ll w$), the current is deflected from its usual way (along the external electric field) due to magnetic field.

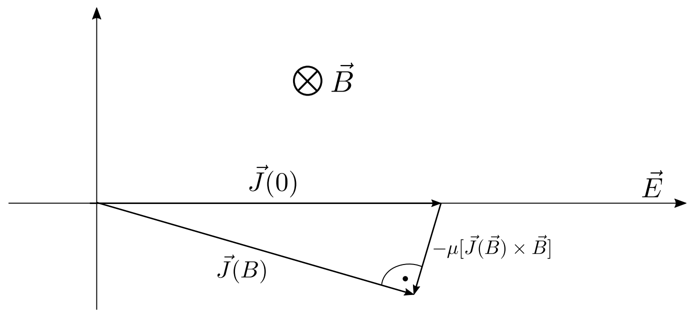

Figure 3.2: Graphical representation of the current defection in a short plate

3.3.3 Magnetoresistance

Magnetoresistance is the property that has a material to change its resistivity when is subjected to external magnetic field. The *magnetoresistance ratio* is the relative change of the resistance of the material when it is under the influence of a magnetic field, it is defined by

$$\frac{\triangle\rho}{\rho} = \frac{\rho(B) - \rho(0)}{\rho(0)} \tag{3.27}$$

In case of short plate ($l \ll w$) the magnetoresistance ratio is given by

$$\frac{\triangle\rho}{\rho} = (\mu B)^2 \tag{3.28}$$

and for the case of a very long plate($l \gg w$)

$$\frac{\triangle\rho}{\rho} = \frac{P_H B^2 cos^2\alpha}{\rho_b} \tag{3.29}$$

where α is the angle between the current and the magnetic field.

The magnetoresistance ratio is always positive for metals, but it is very small. However Bi presents a large magnetoresistance comparable to that in colossal magnetoresistive (CMR) systems. For example, a bulk Bi in a magnetic field of 2T at 295K presents a high magnetoresistance of 110% [6].

3.4 Main characteristics of Hall sensor

3.4.1 Sensor geometry

Equation (3.12) provides us a hint to the sensor's design: it has to be as thin as possible, because V_H is inversely proportional to d. However, it can not be arbitrarily thin, because generally, the signal to noise ratio falls with decreasing d.

Figure 3.3 shows the most popular shapes of Hall sensors. Metal based Hall sensors developed and studied in the Institute of Plasma Physics in Prague are based on variations of design (b). See Fig.3.4.

In general, important features of Hall sensor such as sensitivity or offset depend on geometry. Equation (3.12) was obtained under the assumption that $l \gg w$, this result can be generalized by introducing a *geometrical correction factor* $G_H \in (0, 1)$[24]. Thus, the Hall voltage of a Hall sensor with an arbitrary shape can be expressed as

$$V_H = G_H \frac{R_H}{d} I_H B_y \tag{3.30}$$

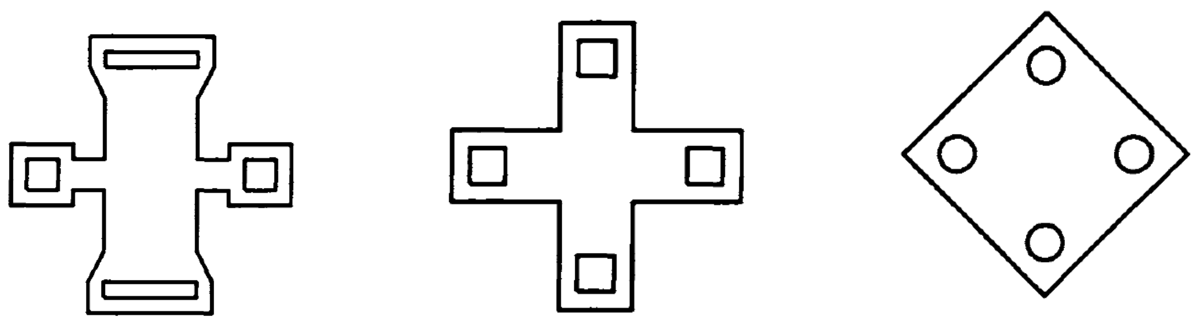

(a) (b) (c)

Figure 3.3: Common Hall sensor shapes: rectangular (a), cross (b), diamond (c)[**?**]

3.4.2 Sensitivity

The quantity that measures the ability of a Hall sensor to provide output voltage for a given magnetic field, is called sensitivity. It can be defined as *absolute sensitivity* and *relative sensitivity*[24]:

- The *absolute sensitivity* is absolute value of the ratio between the Hall voltage and the magnetic field perpendicular to the current I_H

$$S_A = \left| \frac{V_H}{B} \right|_c \tag{3.31}$$

  where C denotes a set of operational conditions such as temperature and bias current.

- The *current related sensitivity* is the ratio of absolute sensitivity and bias current

$$S_I = \frac{V_H}{I_H B} \tag{3.32}$$

$$V_H = S_I I_H B \tag{3.33}$$

  comparing the equation above with 3.30 results

$$S_I = \frac{G_H}{end} \tag{3.34}$$

- The *voltage related sensitivity* is the ratio of absolute sensitivity and voltage which generate the current $I_H (V = I_H \cdot R_{in})$

$$S_V = \frac{S_A}{V} = \frac{V_H}{VB} = \frac{S_I}{R_{in}} = \mu \frac{w}{l} G_H \tag{3.35}$$

$$V_H = S_V V B \tag{3.36}$$

3.4.3 Offset voltage

When a Hall sensor is biased by a current I_H, we would expect that in the absence of a magnetic field the sensor provides zero output voltage. However, the reality is different, there is always present a small output voltage even in the absence of a magnetic field. This voltage is called *offset voltage* and may have different causes such inhomogeneities in the material or misalignment of the sense contacts. In general, the value of the offset voltage tends to be randomly for different sensors.

In the presence of a magnetic field, the output voltage will be given by the sum of the Hall voltage and the offset voltage

$$V_{out} = V_H + V_{offset} \tag{3.37}$$

and in the absence of the magnetic field

$$V_{out} = V_{offset} \tag{3.38}$$

3.4.4 Linearity

A Hall sensor is considered lineal if $V_H \sim I_H B$ hods to a high degree of accuracy for a given temperature. On the basis of equation 3.33 the Hall sensor will be linear if the current related sensitivity does not depend of I_H and B. In order to accuracy the linearity it is defined the non linearity as

$$NL = \frac{V_H(I_H, B) - V_{fit}}{V_{fit}} \tag{3.39}$$

whereV_{fit} is the best linear fit and $V_H(I_H, B)$ is the Hall voltage measured at a current supply I_H and at a magnetic field B. Equation 3.39 tell as how much the data are distant from the fit expressed in percents.

3.5 DC and AC method

When we measure the output voltage of a Hall plate (which is placed in DC magnetic field and it is passing a DC current through the plate i.e. DC method), there are present parasite voltages in the the output voltage. In general the potential V measured by the Hall plate is given by

$$V = V_H + V_E + V_N + V_{RL} \tag{3.40}$$

where V_H is the Hall voltage, V_E is the thermocouple potential due to the Ettingshausen effect, V_N is the potential due to Nernst effect and V_{RL} is the thermocouple potential due to the Righi-Leduc temperature gradient[20]. Then if the direction of the current passing through the Hall plate is reversed, then the output voltage will be given by

$$V_1 = -V_H - V_E + V_N + V_{RL} \tag{3.41}$$

combining the two equation above is ease to prove that:

$$V_H + V_E = \frac{V - V_1}{2} \tag{3.42}$$

If the probes measurig the output voltage are no aligned, then a new component of the offset voltage will be added to the output voltage. Thus

$$V = V_H + V_E + V_N + V_{RL} + V_{offset-1} \tag{3.43}$$

Following the principle of equation (66), changing the direction of the current supply and the magnetic field. It is possible to do four different measurements: V_1 at (+B, +I), V_2 at (+B, -I), V_3 at (-B, -I), V_4 at (-B, +I). Then, combining these four equation results

$$V_H + V_E = \frac{V_1 - V + V_3 - V_4}{4} \tag{3.44}$$

This technique for measurement the Hall voltage is called a "DC-current, DC-field method". The principle is simple, but we have to do four different measurements. If some parameter (such as temperature) changes considerably in the time interval needed to do these four measurements, then the measured Hall voltage could not be reliable.

For this reason it is used AC current and AC field (AC method). Using this this method it is possible to neglect the Ettingshausen effec. A detailed description of this method can be found in [20].

3.6 Requirements of Hall sensor for measurement of magnetic field on fusion devices

At the moment of choosing a Hall sensor in order to measure the magnetic field in a given fusion device, one must take into account, besides others, three fundamental features of the sensor: the *sensibility*, the *operational temperature* and in the case of big tokamaks *neutron fluence resistance*. A good Hall sensor for a given fusion device must:

1. have sufficient sensitivity in order to provide high enough signal to noise ratio.

2. work reliably at the temperatures required by the fusion device.

3. resist the neutron fluence(if there is any), that means that the sensitivity change of the sensor must not exceed same critical value defined by fusion device requirements.

Nowadays semiconductor based Hall sensors are very common and are well studied, most of them satisfies the first criterion, However, in the case of big Tokamaks the second an third criterion are difficult satisfied. Table3.1 shows the temperature and neutron fluence requirements that must satisfy a sensor in ITER and DEMO, while table 3.2 shows the parameters of some interesting commercially available Hall sensors. Obviously any of this commercially available Hall sensors can be used in ITER.

	$T_{op}[°C]$	T_s $[°C]$	F_t $[cm^{-2}]$
ITER	$100 - 150$	220	10^{18}
DEMO	Several hundred	Several hundred	$> 10^{20}$

Table 3.1: Some parameters for ITER and DEMO reactors. T_{op} is the operational temperature, T_s is the survival temperature and F_t is the total neutron fluency.

Type	Producer	Material	T_{max} [°C]	$S[mV/T]$	$I_{H-max}[mA]$
A1322LUA	Allegro	not specified	150	31250	not specified
HGT-3010	Lakeshore	InAs, bulk highly doped	100	10	100
HGT-3030	Lakeshore	InAs, bulk low doped	100	100	100
HS-100	F. W. Bell	InAs thin film	185	240	30
GH-800	F. W. Bell	GaAs bulk	175	1000	5

Table 3.2: Parameters of different Hall sensors [12]. T maximal operational temperature;S sensitivity; I_{max} maximal control current

3.7 Metal based Hall sensors

Unlike semiconductor Hall based sensor, metal based ones are more compatible with high temperatures and radiation environment. Therefore, they have a good perspective to be part of the magnetic diagnosis in big fusion reactors. However, the investigation of the properties of metals, such as Hall sensors, started just few year ago. Therefore, it is necessary to characterize their properties, such as sensitivity, linearity, signal to noise ratio, etc. at big fusion devices environment. Particularly, at ITER ex-vessel SSMS environment. This bachelor thesis is focused on study of these properties for bismuth based Hall sensors.

3.7.1 Material selection

Metal Hall sensors have significantly smaller sensitivity than semiconductors ones due to the fact that Hall coefficient (consequently the sensitivity see Eq.3.34) is inversely proportional to free electron density (see equation 3.10). Most of metals present relative same order of degree of sensitivity. An exception is the bismuth which have the biggest sensitivity (approximately four orders bigger). Table3.3 provides a comparison between sensitivities of some metals of interest at $d = 1\mu m$ and $G_H = 1$. Clearly bismuth is the most attractive one. However, the possible applications of bismuth are limited by its melt point (275.5 °C). According with table 3.2, bismuth could be used in ITER.

Metal	Sensitivity R_H/d [$\mu V/A/T$]
Cu	55
Bi	$\sim 10^5$
Al	34
Pt	23

Table 3.3: Sensitivity of some metals of interest: copper, bismuth, aluminum, and platinum at $d = 1\mu$ and $G_H = 1$[7]

3.7.2 Design and construction technology

The hard environment of ITER ex-vessel considerably limits the kind of material (besides the sensing layer material) that can be used in design of a Hall sensor, the technology paradigms can be summarized as follows[7]:

- Ceramics and metals only (no plastics, glues ect)

- Bonded electrical contacts (no crimp contacts, soldering, etc)
- Low activation materials

A metal Hall sensor is formed by five elements: subtract, shape thin sensing layer, contact areas, encapsulation, and output wires. An extensive description of each element can be found in [29].

Fig.3.4a shows a schema and photography of a bismuth based sensors type K1 (BiK1), this sensor has a thickness about 4.5 μm and Al_2O_3 ceramic subtract. Fig. 3.4b is a "+" design used in [7].

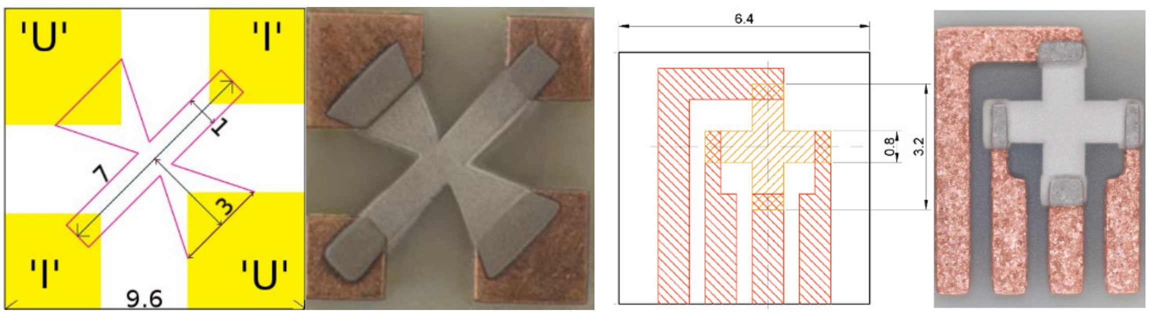

(a) [29]All dimensions are expressed in mm

(b) [7]

Figure 3.4: Bismuth based sensors design, K1 design (a), "+" design (b)

3.7.3 FISPACT activation analysis

As mentioned above a magnetic sensor in big tokamaks will be subject to high neutron fluence and it is important to know the activation level of sensor's material. It is possible to do a real experiment. However, using same simulation tool, such a FISPACT activation code, is cheaper and faster. Table 3.4 summarizes the results obtained by FISPACT simulation when a $1\,\mu m \times 6\,mm^2$ samples (of different metals) are subjected to different total neutron fluences.

Total neutron fluence[cm^{-2}]	Activity			
	Cu [Bq]	Bi [Bq]	Pt [Bq]	Al [Bq]
1.3×10^{18}	2.9	399	9150	0
5.4×10^{19}	379	9080	1.5×10^6	0
1.1×10^{20}	546	1.3×10^5	1.7×10^6	0

Table 3.4: Results obtained by FISPACT simulation. $1\,\mu m \times 6\,mm^2$ samples of Cu, Bi, Pt, Al are subjected to different neutron fluences [29]

Chapter 4

EXPERIMENTAL EQUIPMENT

As discussed in section 3.7, metal based Hall sensors present a good perspective to be part of the magnetic diagnosis of big fusion reactors due to their ability to measure the magnetic field directly. For example, Hall sensors based on cooper or bismuth. However, the investigation of the properties of these metals started just few year ago. Therefore, it is necessary to characterize their properties, such as sensitivity, linearity, signal to noise ratio, etc. at big fusion devices environment. Particularly, at ITER ex-vessel SSMS environment. As a consequence, the Institute of Plasma Physics in Prague had developed a special test-bench in order to characterize metal Hall sensors at ITER ex-vessel temperature environment.

This equipment is able to characterize the parameters of steady state magnetic sensors at temperatures up to 300°C in the presence of a reasonable homogeneous magnetic field up to 500 mT. The calibration circuit is schematically shown in figure 4.1.

4.1 High-temperature coil

The core of the experimental equipment is the *High-temperature coil* . It is based on Helmholtz coil concept i.e. two coaxial winding packs separated by distance r (see figure 4.3). The wire is made of copper and have a rectangular cross section of $1.5 \times 3.3\,mm^2$ insulated by Kapton. This cross section is the result of a rigorous analysis of the dimensional parameters, which have been done in order to maximize the magnetic field. The rest of the optimized dimensional parameters are listed in table 4.1. The High-temperature coil is able to generate a magnetic field up to $500\,mT$ with a good homogeneity. At the distance of 5 mm of the coil's geometrical center, the change of magnetic field is 0.2% and 0.4% in radial and axial direction respectively, see figure 4.2. The calibration factor of the High-temperature coil is $B/I = 7.40\,mT/A$ [18].

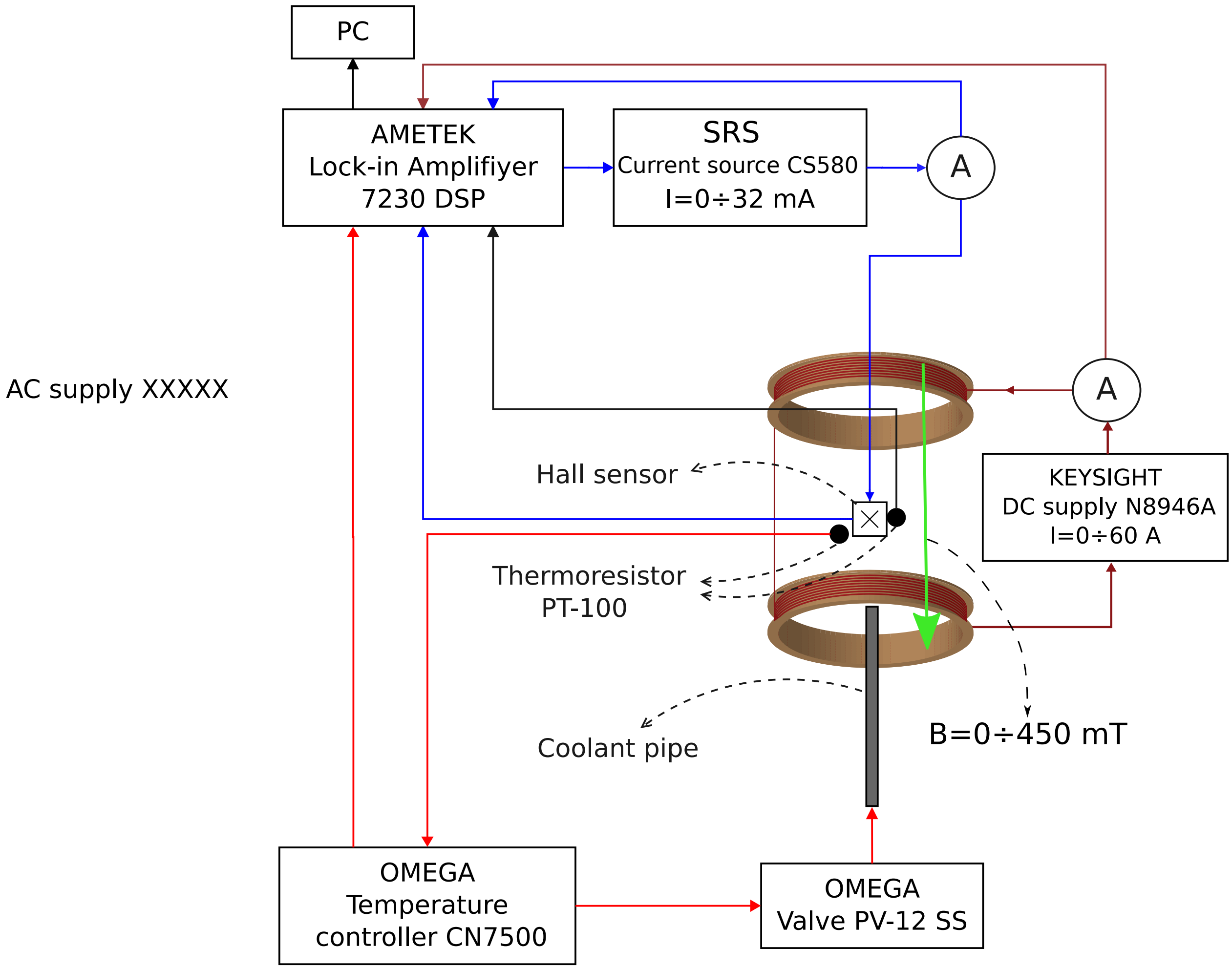

Figure 4.1: Schematic of the Hall sensor's calibration set-up.

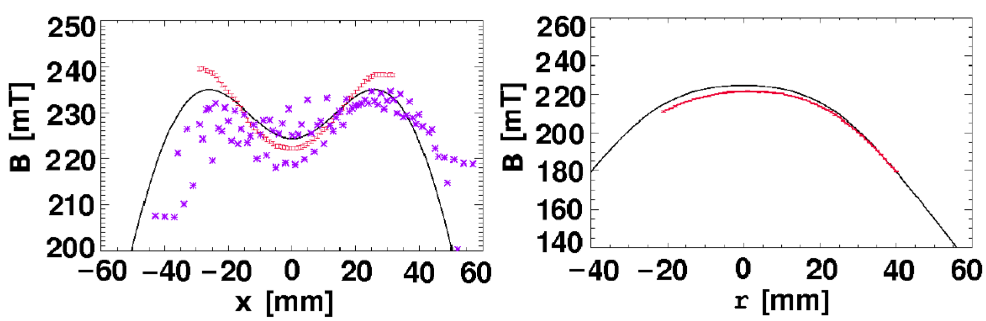

Figure 4.2: Comparison of magnetic field profile in axial(left) and radial (right) direction. Theoretical value(black solid line), measured on cold coil(red bars), and measured on hot coil (violet stars)[18].

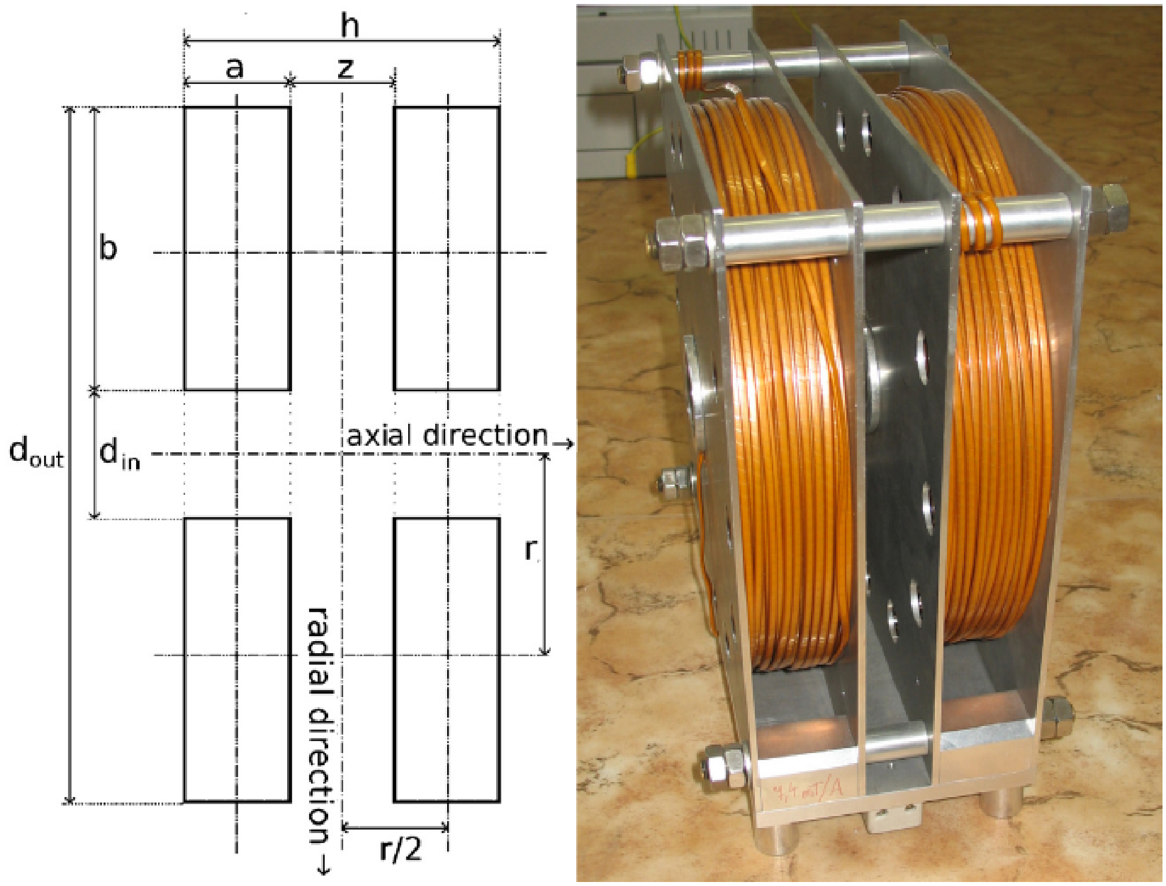

Figure 4.3: Left – overall geometrical set-up of the designed coil based on Helmholtz coil concept. Right – photograph of the high-temperature coil [18].

Name of parameter	Value of parameter
Size of wire $d_{wa} \times d_{wr}$	1.5 × 3.3 mm
Insulation/thickness	Kapton/0.23 mm
Size of winding pack $a \times b$	38.8 mm × 96.9 mm
Radius of the coil r	74.0 mm
Inner space $d_{in} \times z$	51.1 mm × 35.2 mm
Outer coil size $d_{out} \times h$	244.9 mm × 112.8 mm
Number of windings N (overall)	1232
Magnetic field in center B	224.5 mT
Weight of winding m_{Cu}	25.3 kg
Resistance of winding R	3.868 Ω
Power deposited in coil P	3481.0 W
Heating rate	0.36 °C/s
Inductance L	158.6 mH

Table 4.1: Parameters of optimized High-temperature coil at supply current I=30 A

4.2 Test bench

Synchronous detection is used in order to avoid parasitic voltages in the output of the Hall sensor. The high-temperature coil is biased by a DC current using [KEYSIGHT Autoranging system DC supply] in the range of $I_B = 0 \div 60\ A$, generating a magnetic field of $B = 0 \div 450\ mT$.

A metallic Hall sensor is inserted into high-temperature coil and a AC current is driven through the Hall sensor in the range of $I = 0 \div 35\ mA$, by [SRS Voltage controlled current source CS580]. As a consequence of the Hall effect, the Hall sensor provides an output voltage (see section 3.4.3). In order to reduce the noise as much as possible, the output voltage is measured by [AMETEK Look-in Amplifier 7230 DSP] which is locked to the frequency of the biasing current.

As was said above, we are interested in testing the properties of the Hall sensor at temperature close to 200°C, for this, an external source of heat is not necessary since the high temperature coil provides enough heat due to the joule effect. The Hall sensor also provides heat due to the same effect but the dominant source is the high temperature coil.

If it is necessary to cool the Hall sensor, from temperature T_2 to T_1(where T_2 and T_1 are preselected values) it is used a pressurized air flow, which is regulated by a temperature control circuit. This temperature control circuit consist of three parts: [SIEMENS PID temperature control] which is connected to electronically controlled [Omega proportioning valve PV-12 SS] and the [thermoresistor PT-100] providing the temperature of the tested sensor. The whole circuit is connected to a PC enabling to set up all the parameters of the experiment. Additionally, ammeters are connected for visual control.

The whole test bench is shown in figure 4.4.

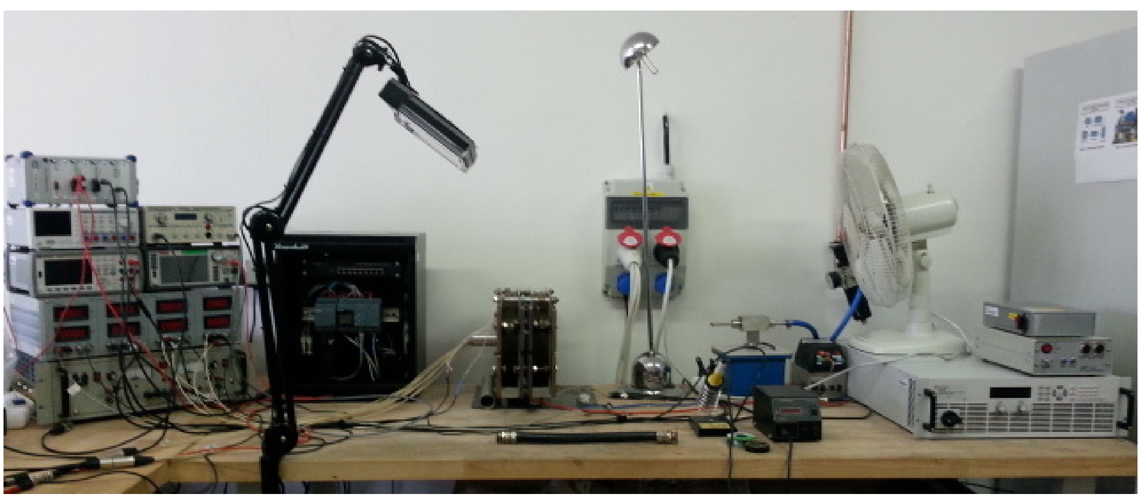

Figure 4.4: Photograph of the test bench

4.3 Output signal processing

As seen in section (3.4.3), the offset voltage is always present in the output voltage of the Hall sensor. Therefore, the current supply to the high-temperature coil is switched on and off at preselected intervals Δt allowing us to identify the value of the offset voltage and consequently the real value of the Hall voltage. Typically, it is switched every 2 seconds and in previous versions of the test bench it was done every 10 seconds.

The output voltage of the Hall sensor at switched-on time t_{ON} (i.e. at non zero magnetic field) is given by the sum of the real Hall voltage and the offset voltage

$$V_{out}(t_{ON}) = V_H + V_{offset} \tag{4.1}$$

If the switch-time interval is $\triangle t$, then the output voltage at switched-off time $t_{OFF} = t_{ON} + \triangle t$ (i.e. at zero magnetic field) is given by

$$V_{out}(t_{ON} + \Delta t) = V_{offset} \tag{4.2}$$

Finally the Hall voltage is given by

$$V_H(t_{ON}) = V_{out}(t_{ON}) - V_{out}(t_{OFF}) \tag{4.3}$$

Figure 4.5 shows an example of the output voltage of the Hall sensor, the top panels correspond to a measurement, where the supply current to the high-temperature coil was switched on and off every ten seconds, while the bottom panels every two seconds. In the measurement of Fig.4.5a the upper line denotes the offset voltage (i.e. the output voltage at zero magnetic field) and the bottom line represents the output voltage at non zero magnetic field, unlike the measurement of Fig.4.5b, where the upper line denotes the output voltage at non zero magnetic field and the bottom line represents the offset voltage.

Figure 4.5a clearly shows many data prints measured at intermediate states, it is because in previous version of the test bench, the synchronization technique between the switched on and off current and the data measurement was not as optimized as now.

If the temperature over the experiment rises relatively fast, the choice of ten second as a switched interval would present some issues. We will be able to identify reliably the value of the Hall voltage only once in every 10 seconds, it reduces considerably the resolution in temperature. Therefore, two seconds as a switched interval is more attractive, if we are interested in temperature dependence of same characteristic such as sensitivity.

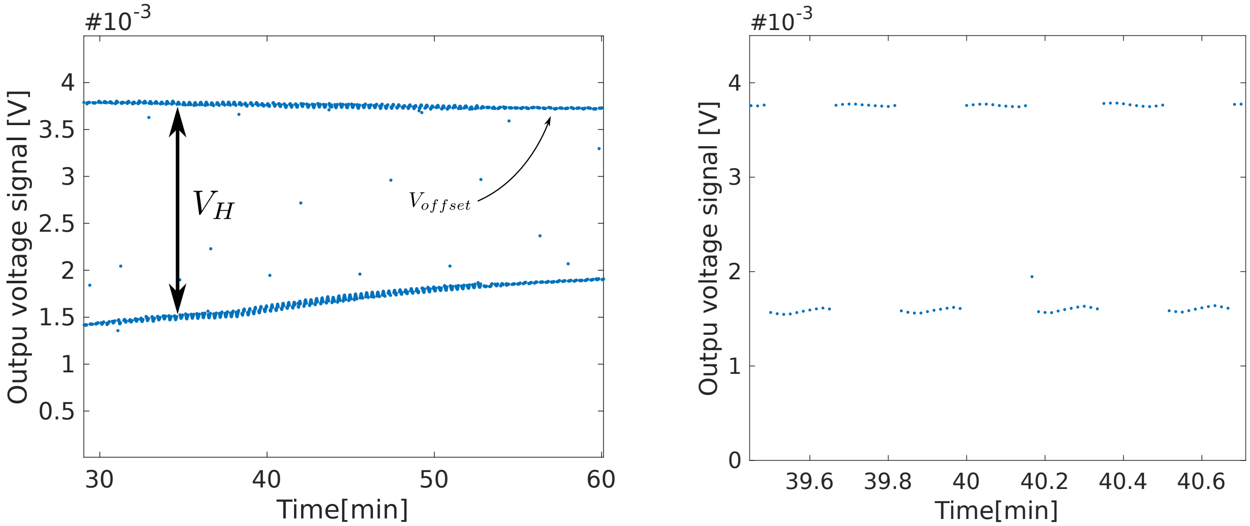

(a) Sensor BiS3K1, temperature 95°C, current 22 mA

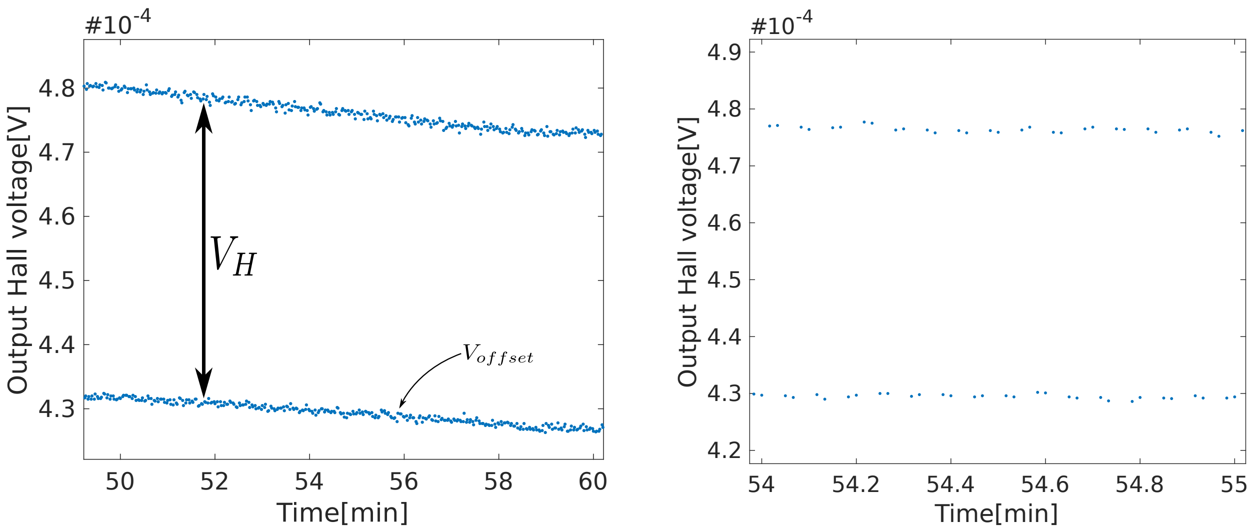

(b) Sensor BiS7K1, temperature 200°C, current 5.3 mA

Figure 4.5: Comparison of output voltage periodically switched on and off (a) every 10 seconds. (b) every 2 seconds. Right panels are the respective zooms at a time interval of one minute.

Chapter 5

RESULTS

5.1 Measured quantities

To sum it up, for the characterization of a Hall sensor, it have been measured four different quantities simultaneously:

- *AC current to the Hall sensor*, supplied by [SRS Voltage controlled current source CS580] in the range of $I_H = 4 \div 32\ mA$.
- *DC current to the high-temperature coil*, supplied by [KEYSIGHT Autoranging system DC supply], in the range of $I_B = 0 \div 60\ A$. Then, the magnetic field is obtained by using the calibration factor $B/I_B = 7.40\ mT/A$. Thus, the magnetic field is in the range of $B = 0 \div 450\ mT$.
- *Temperature of the sensor*, measured by [PT-100 thermoresistor].
- *Output Hall voltage*, it is the output voltage of the Hall sensor and it is measured by [AMETEK Look-in Amplifier 7230 DSP] which is locked to the frequency of the biasing current to the Hall sensor.

All these quantities are shown in figure 5.1 with the same time axis for a measurement with a Hall sensor BiM5C6. The current supply to Hall sensor was set up to remain constant over the experiment ($I_H = 4\ mA$), whereas the current supply to the high-temperature coil was switched on($I_B = 37\ A$) and off ($I_B = 0$) every two seconds using the PC. During the experiment, the temperature rose from 30 °C to 100 °C, this rise was caused primarily by the heat generated by the high temperature coil. The offset voltage increased just 1.85% of the initial value (Fig.5.1 fourth panel - bottom line) while the Hall voltage clearly drops with the temperature (Fig.5.1 fourth panel - V_H = difference between upper line and bottom line). This drop was approximately 50% of the initial value.

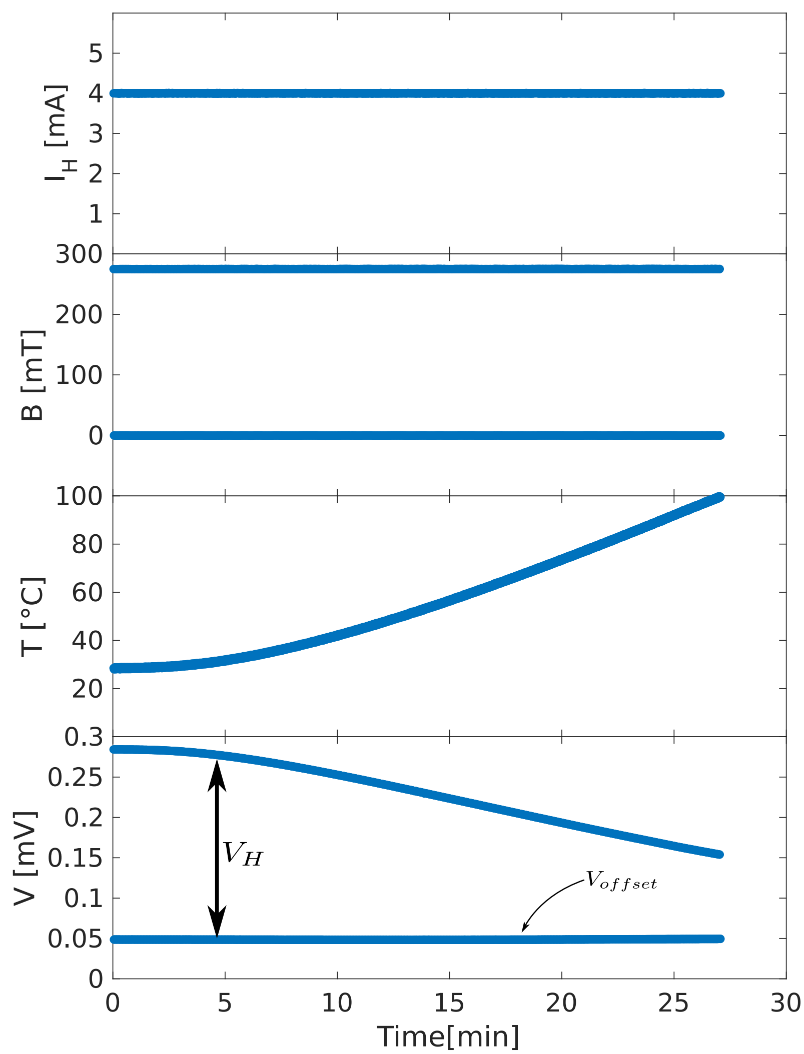

Figure 5.1: Measured quantities of Hall sensor BiM5C6. Panels from top to bottom: I_H - AC current Supply to Hall sensor, B - magnetic field generated by the high-temperature coil calculated from biased DC current by factor $B/I_B = 7.40\, mT/A$, T - temperature of the Hall sensor, V - output voltage of the Hall sensor.

Figure 5.2 illustrates the performance of the temperature control circuit described in section 4.2. Using the PC, we where able to set up the minimal temperature $T_{min} = 35°C$ and the maximal temperature $T_{max} = 120°C$. The experiment started with a temperature of the Hall sensor of 55°C and the process was totally automatized. When the temperature of the sensor reached the maximal selected value, the circuit automatically opened the [valve PV-12 SS] and controlled the pressurized air flow until the temperature decreased to the minimal selected value, then the circuit closed the [valve PV-12 SS] and the process started again. Note that Fig.5.2 - bottom panel illustrates more clearly the dependence of the Hall voltage on temperature.

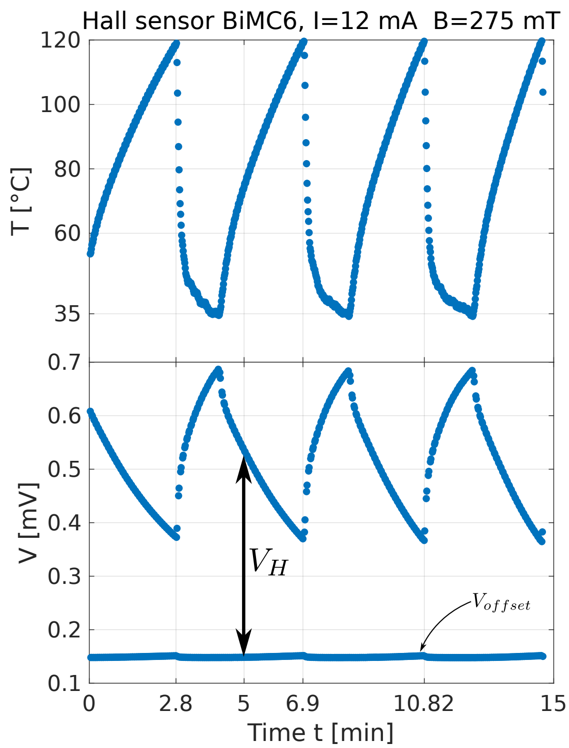

Figure 5.2: Performance of the temperature control circuit. Preselected values: $T_{min} = 35°C$, $T_{max} = 120°C$. Top panel: T - temperature of the Hall sensor. Bottom panel: V - output voltage of the Hall sensor.

5.2 Offset

Figure 5.3 shows the offset voltage of Hall sensor BiM5C6 as a function of temperature. Each curve correspond to a different measurement with different settings of AC current supply to the Hall sensor. The offset voltage presents a small quadratic increase with the temperature for all values of current. It is difficult to see the quadratic dependence in Fig.5.3, but figure 5.4a illustrates a zoom for the especial case, when the current was $I = 34mA$. However, the offset voltage change did not exceed the 2.5% of the initial value in all cases. On the other hand, figure 5.3 clearly shows that the offset voltage increase with the biased current to Hall sensor. In this case, the dependence is linear as can be seen in figure 5.4b, the data are almost superposed for different value of temperature $T_1 = 65°C$, $T_2 = 85°C$ and $T_3 = 115°C$, because as stated above the change of the offset voltage did not exceed the 2,5%.

Although the offset voltage of the BiM5C6 slowly changes with temperature, it increases quadratically; it is not the case of the sensor BiS7K1, which exhibits a slow linear drop with temperature (see Fig.5.5), this drop is about 0.04%/°C.

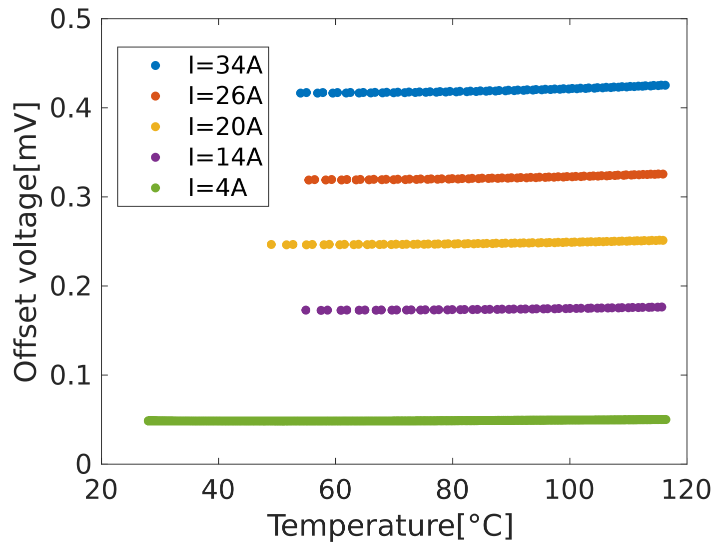

Figure 5.3: Offset voltage as a function of temperature of Hall sensor BiM5C6 measured at different AC current supply to Hall sensor.

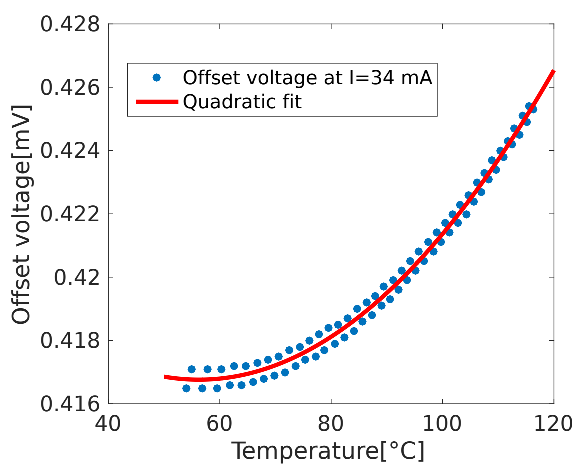

(a) Offset voltage vs temperature

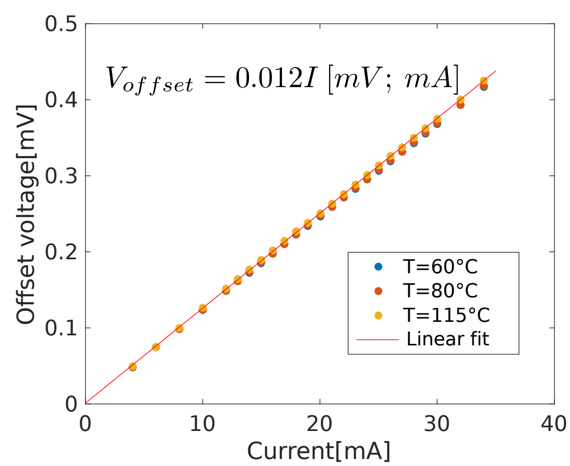

(b) Offset voltage vs current

Figure 5.4

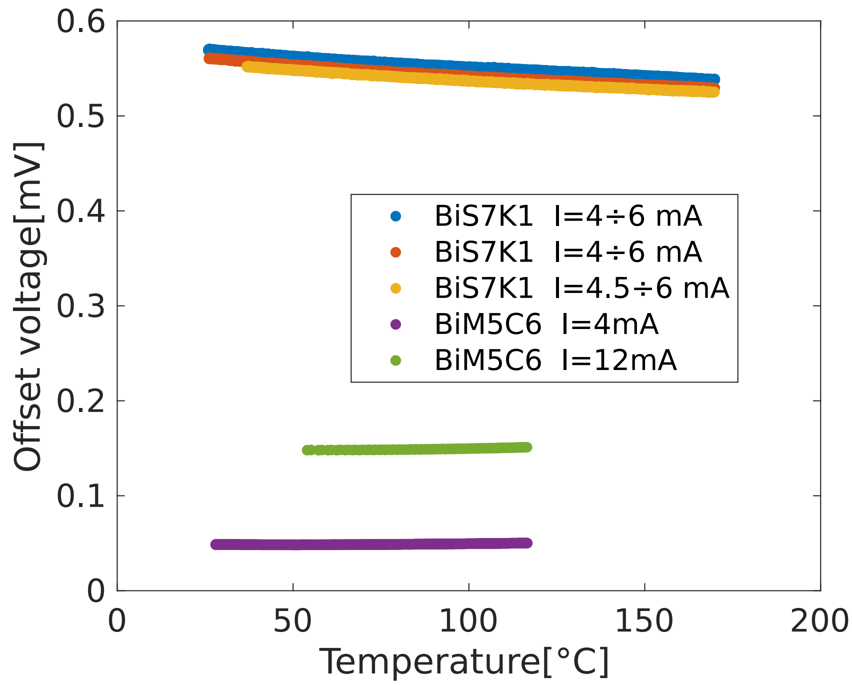

Figure 5.5: Offset voltage as a function of temperature of Hall sensor BiS7K1 and BiM5C6

5.3 Sensitivity

For the characterization of the sensitivity we used Hall sensor BiS7K1 with setting parameters: AC current supply to hall sensor $I_H = 4 \div 6\,mA$ and DC current supply to high-temperature coil $I_B = 34\,A$. Thus, it was calculated the current-related sensitivity using equation 3.32, which we repeat:

$$S_I = \frac{V_H}{I_H B} \tag{5.1}$$

Different measurements showed that the sensitivity decreases with rising temperature, see Fig.5.6. This behavior can be relatively well fitted by a third order polynomial. However, the higher the temperature, the greater the linear dependence. The temperature interval of some measurement was cut in order to illustrate the superposition of the sensitivity of different measurements in figure 5.6. The sensitivity decrease at temperature of 200°C was 71% of initial value at 26°C, it implies that a bismuth based Hall sensor will need additionally a temperature measurement included in the probe circuit in order to be used as a magnetic sensor in fusion devices.

Figure 5.7 shows the output voltage of a Hall sensor BiM5C6 at current supply $I_H = 15\ mA$, it is clearly seen an erratic behavior after 20 min. It is a sign that the sensor damaged.

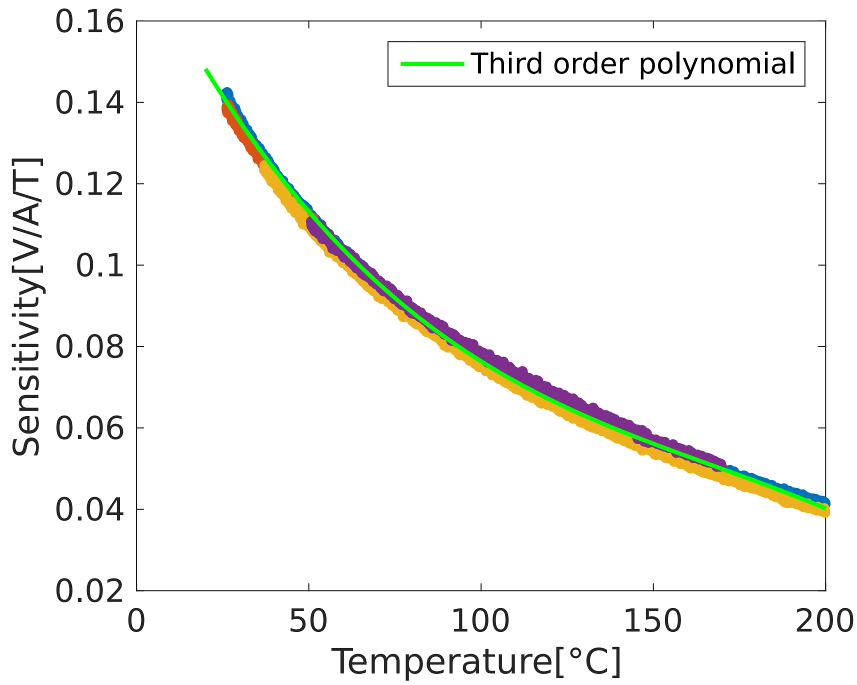

Figure 5.6: Dependence of sensitivity of Hall sensor BiS7K1 on temperature. Different colors denote different measurements.

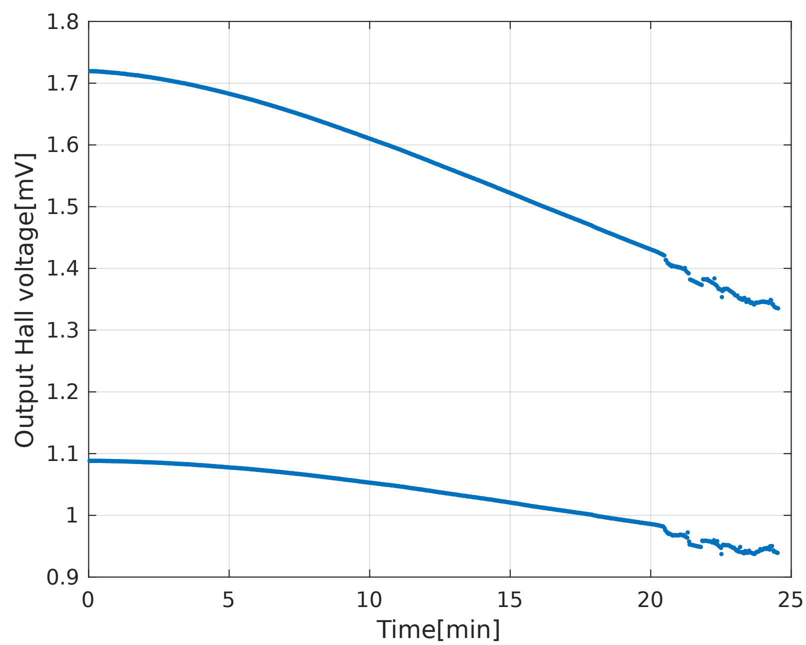

Figure 5.7: Output Hall voltage of Hall sensor BiM5C6. Current supply to sensor $I_H = 15\,mA$, magnetic field $B = 275\,mT$

5.4 Linearity

5.4.1 Hall voltage vs current

For this experiment it was used the Hall sensor BiM5C6 and the current supply to high-temperature coil was switched on ($I_B = 37A$) and off ($I_B = 0$) every two seconds. The temperature control circuit was set up at ITER relevant temperature: $T_{min} = 50°C$ and $T_{max} = 120°C$. Then, we have measured all quantities from section 5.1 with current supply to Hall sensor $I_H = 4\ mA$. When the temperature reached T_{max}, the temperature control circuit started colling and the first measurement finish. After that it was set-up a higher current I_H and the measurement started again. The process was repeated for current in the range $I_H = 4 \div 34\ mA$. The dependence of the Hall voltage on the current is showed in figure 5.8 for different temperatures. The behavior presents a linear dependence where the slope decreases with rising temperature. A more accurate analysis can be done by calculating the non linearity (3.39), it is shown in figure 5.9.

When the magnetic field is constant, linear dependence of Hall voltage V_H on current I_H implies that the current related sensitivity is constant for a given temperature regardless of the value of I_H (see Eq. 3.32). In other words, V_H depends linearly on I_H if and only if the current related sensitivity is constant for a given temperature.

In the case of figure 5.9, the non linearity did not exceed the 4% for current I_H bigger than $6\,mA$; however, the non linearity is about 12.5% and 8% for current $I_H = 4mA$ at temperature of 65°C and 85°C respectively. These deflections from linearity are considerably big and have direct consequence in the current related sensitivity as shown in fig. 5.10. It is clearly seen the discrepancy between the sensitivity at $I_H = 4\ mA$ and the sensitivities at $I_H \geq 6\ mA$; additionally, the latter ones present a small concavity at the starts, while the sensitivity at $I_H = 4mA$ presents only convexity. A completely independent experiment using the same sensor (see figure 5.11) showed that, the correct sensitivity in Fig.5.10 is the one that corresponds to $I_H = 4\ mA$. It implies that the correct fit at 65°C in Fig.5.8 would be the dashed black line.

The reason why the other sensitivities are displaced to left in Fig. 5.10 is related to the temperature measurement technique and to the time interval of each measurement (at different current).

The PT-100 thermoresistor is attached to sensor providing the temperature. On the one hand, the temperature control circuit reduced the temperature relatively fast (1.5 min) from maximum preselected value (120°C) to nominal value (50°C) using a flow of pressurized air, after that for $I_H \geq 6\ mA$ the temperature increased to the maximal value in only 3 min. If the thermoresistor is placed between the sensor and the flow of air, then there is no enough time to reach the thermal equilibrium between the thermoresistor and the sensor. On the other hand, current I_H heats the Hall sensor from inside and it is also needed enough time to reach thermal equilibrium. For these reasons, the measured Hall voltage actually corresponds to a higher temperature.

This issue can be solved using the Hall sensor itself as a thermometer, it is possible thanks to the fact that the resistivity of bismuth is proportional to the temperature. currently the team of the Institute of Plasma Physic in Prague is working to use this method for temperature measurement.

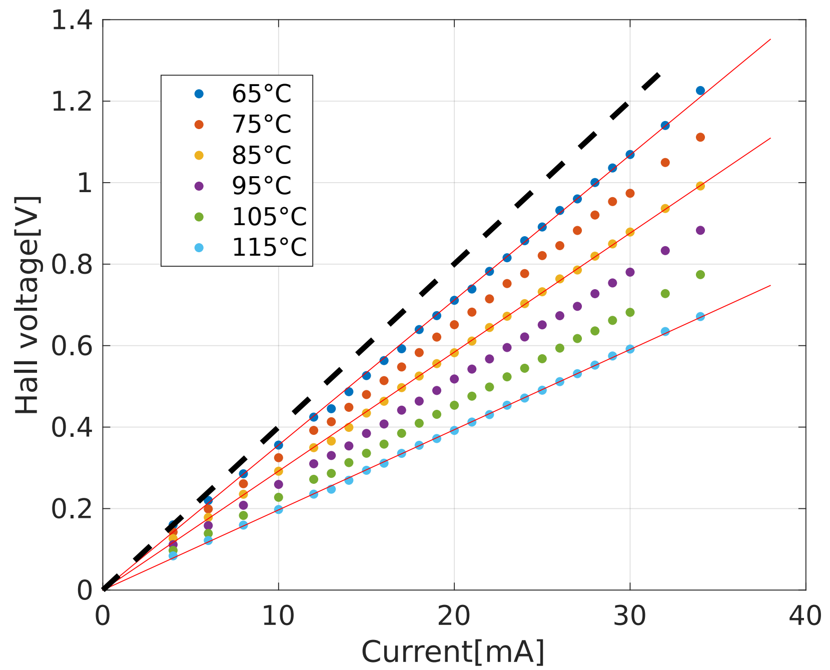

Figure 5.8: Hall voltage as a function of current for different temperatures. Dashed black line - theoretical correct fit corresponding to temperature 65°C.

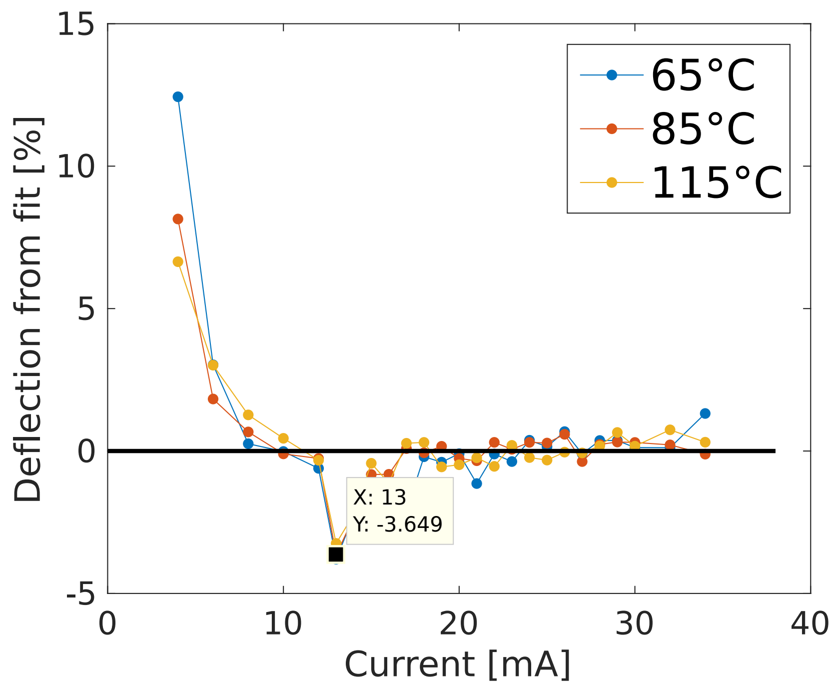

Figure 5.9: Non-linearity of Hall voltage, $100 \times [(V_H(I) - V_{H,fit}(I))/V_{H,fit}(I)]$ vs current. Temperature 115°C and 105°C. Magnetic field 175 mT.

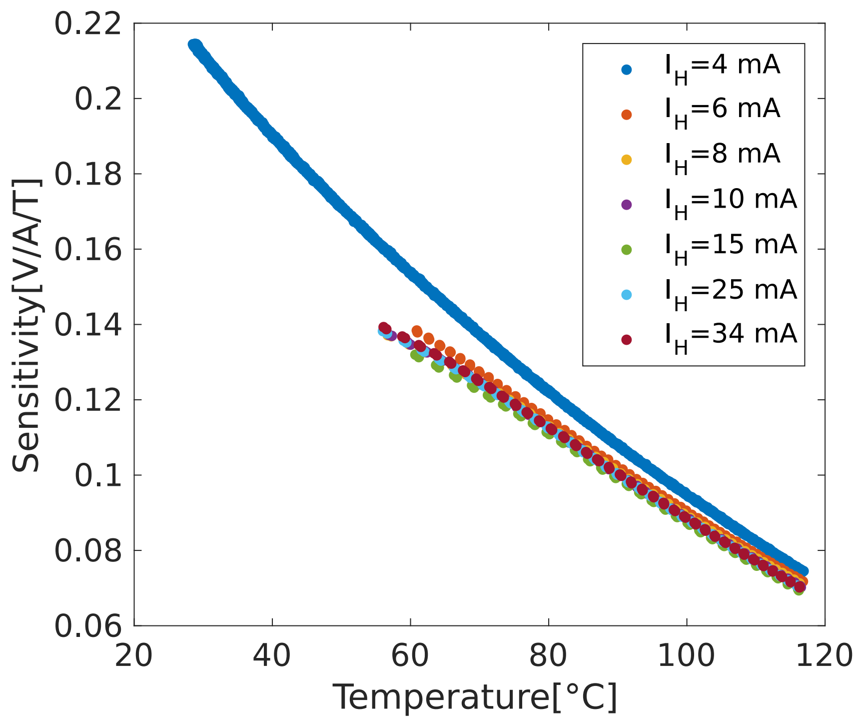

Figure 5.10: Dependence of sensitivity of Hall sensor BiM5C6 on temperature. Each curve was obtained from different measurement at different value of current $I_H = 4 \div 34\, mA$

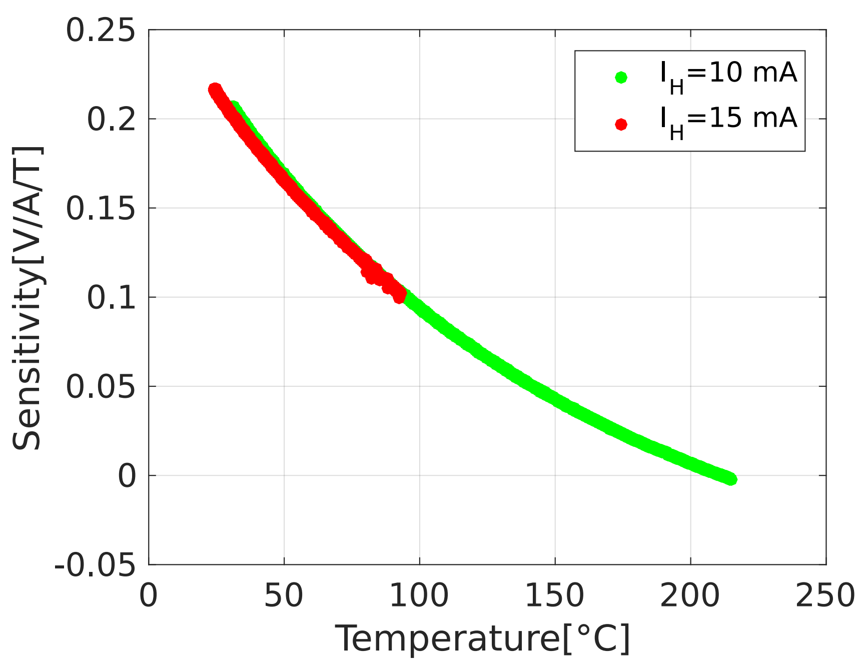

Figure 5.11: Sensitivity of Hall sensor BiM5C6

5.4.2 Hall voltage vs magnetic field

For this experiment, it was used a Hall sensor BiM4C1. The current supply to high-temperature coil was set up to increase from 0 to 60 A in steps of 1 A every two second, while the time switched on and off interval was $\triangle t = 1\,s$. Over all experiment the current supply to Hall sensor $I_H = 4\,mA$ remained constant and the mean temperature was 26°C with a standard deviation of 0.026°C. Figure 5.12 shows the dependence of the Hall voltage on magnetic field. Although, it can be said that the non linearity did not exceed the 10%, the non-linearity decreases almost monotonically with the magnetic field to 1.2% in negative direction as seen in figure 5.13. This behavior suggests that the dependence of V_H on B is nonlinear. If the dependence was linear, then the nonlinearity would fluctuate around 0. Very recent research [7] confirms that the dependence of V_H on B is no linear, additionally the in the region $B = 1 \div 7\,T$ the dependence may considered as linear. As a result, function in the form:

$$V_H = aB + b \cdot atan(cB) \tag{5.2}$$

can be use to fit the data[7]. The result is showed in Fig.5.13. It is clearly seen that Eq. (5.2) fit the data fits the data quite accurately for magnetic field $B > 0.1\,T$ (the deflection from the fit do not exceed the 0.3%). A further point worth noting is that for $B < 0.5\,T$ (i.e. in the region of our experiment) the data can be fitted by a second order polynomial in the form:

$$V_H = a_0 B + b_0 B^2 \tag{5.3}$$

Fig. 5.10 shows how this simple fit almost overlap the fit calculated using Eq.5.2. This fact may suggest that the argument of arc tangent function in Eq. (5.2) is not aB. Instead, it could be aB^2. Thus:

$$V_H^* = aB + b \cdot atan(cB^2) \tag{5.4}$$

and for $cB^2 < 0.5\,T$ holds:

$$V_H^* \approx aB + bcB^2 = a_0 B + b_0 B^2$$

which is in concordance with (5.3). A comparison using of fit using (5.2) and (5.4) is showed in figure (5.14).

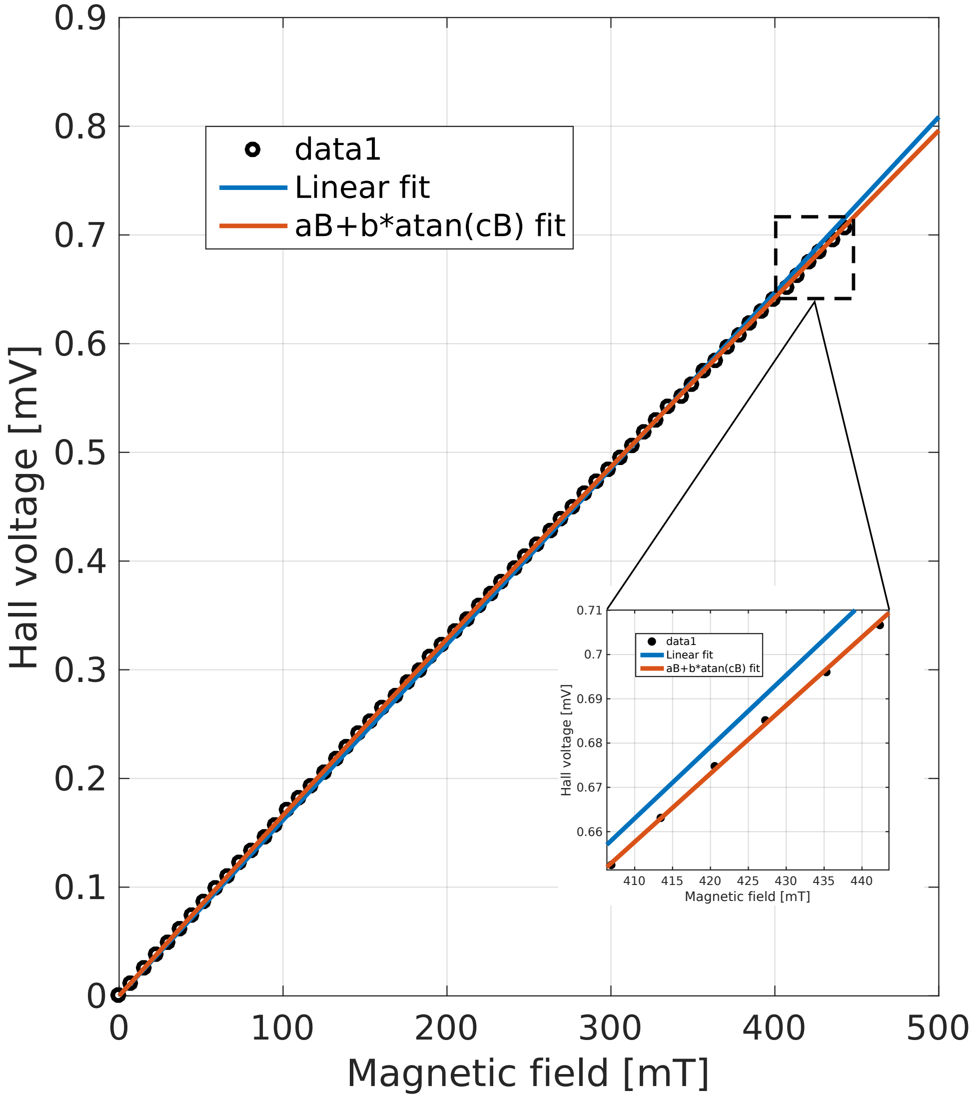

Figure 5.12: Hall voltage vs magnetic field at a temperature of 26°C.

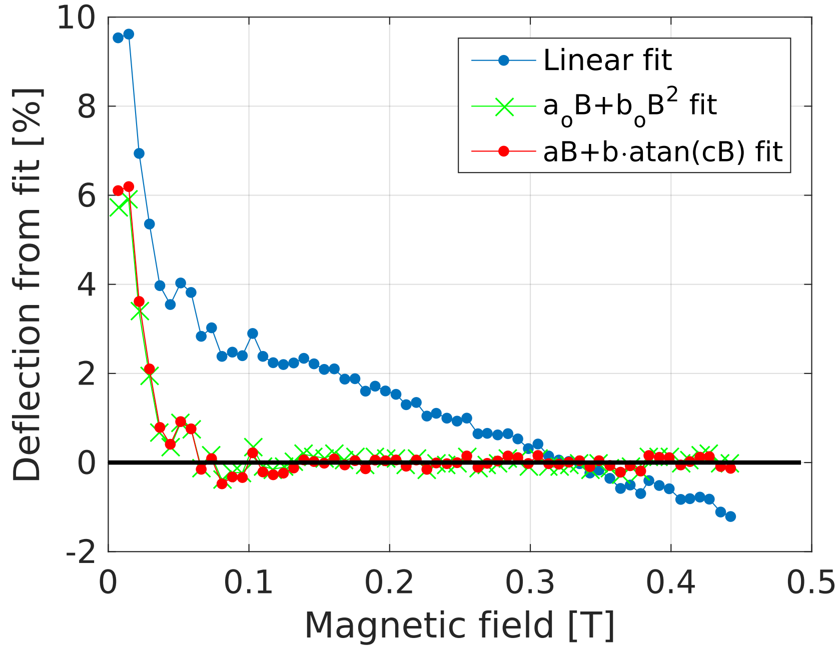

Figure 5.13: Deflection of Hall voltage from the fitted curve, $100 \times [(V_H(B) - V_{H,fit}(B))/V_{H,fit}(B)]$ vs magnetic field at a mean temperature of 26.8°C with standard deviation of 0.026°C; Hall sensor BiM4C1.

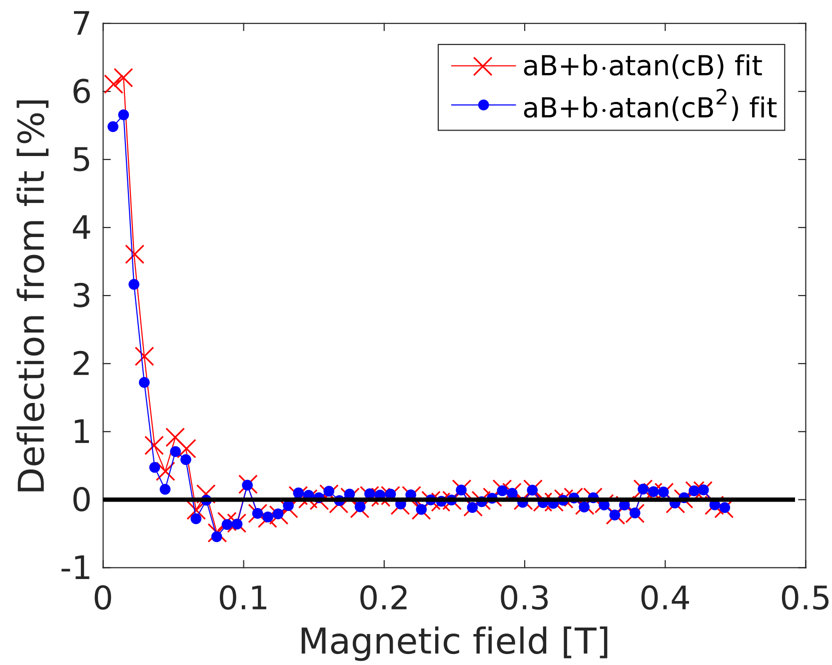

Figure 5.14: Comparison of fit using equation (5.2) and (5.4). $100 \times [(V_H(B) - V_{H,fit}(B))/V_{H,fit}(B)]$ vs magnetic field

5.5 Amplification of the offset-cancellation electronics

The offset-cancellation electronics was also used to measure the Hall voltage in the experiment described in the previous selection. A comparison between the Hall voltage obtained by removing the offset and the Hall voltage measured by the offset-cancellation electronics is shown in figure 5.15a. The data showed that the output-to-input voltage ratio of the offset-cancellation electronics is 1145:1. It is illustrates in figure 5.15b.

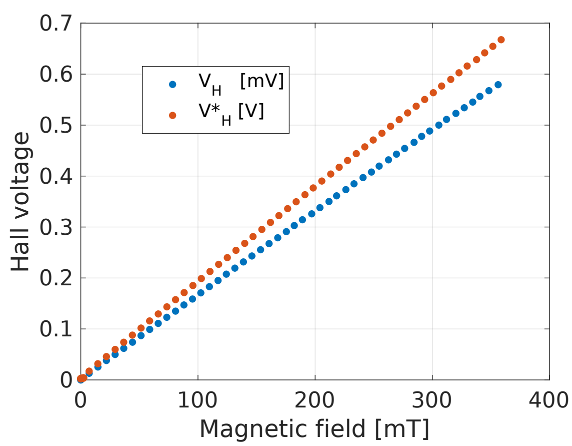

(a)

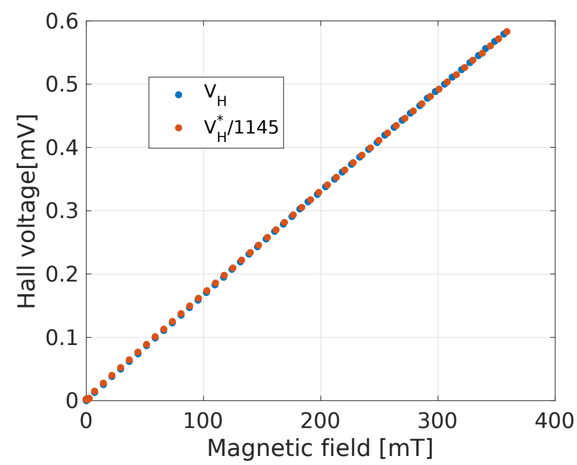

(b)

Figure 5.15: Hall voltage of sensor BiM4C1, at $I_H = 4\ mA$, V_H - Hall voltage obtained by removing the offset, V_H^* - output voltage of the offset-cancellation electronics

Chapter 6

Summary and conclusions

The most common method for measurement of magnetic field on fusion devices is based on magnetic induction coils. Using this method, it is possible to measure the derivative on time of the magnetic field. Subsequently, using analog or numerical integration, it is possible to determine the absolute level of magnetic field. However, if there are present relevant drifts, noise or pick-ups of other magnetic field component, the proper integration becomes a difficult task. For this reason, it is attractive to use a different method which could measure the absolute value of magnetic field itself and not its derivative. A metal Hall sensor can be used for this purpose. However this is a relative new field and the properties of metal Hall sensors at big-reactors(such as ITER or DEMO) environment must be further studied. This bachelor thesis is focused on the characterization of metal Hall sensors based on bismuth.

The Institute of Plasma Physics in Prague had developed a special test-bench in order to characterize metal Hall sensors at ITER ex-vessel temperature environment. This equipment is able to characterize the parameters of steady state magnetic sensors at temperatures up to 300°C in the presence of a reasonable homogeneous magnetic field up to 500 mT (See Fig.4.1 and Fig. 4.4).
The results described in detail in chapter 5 can be summarized as follows:

- Bismuth based Hall sensors was successfully tested using the test bench developed by Institute of Plasma Physics in Prague.
- The value of the offset voltage of sensor BiM5C6 increased quadratically with increasing temperature. However, it did not exceed the 2.5% of its initial value (see Fig.5.4a), while the offset voltage of sensor BiS7K1 exhibits a slow linear drop about 0.04%/°C (see Fig. 5.5); see section 5.2.
- The sensitivity of sensor BiS7K1 decreases with rising temperature. A third order polynomial can fit this curve (see Fig. 5.6). The sensitivity decrease at temperature of 200°C was 71% of initial value at 26°C. It implies that a bismuth based Hall sensor will need additionally a temperature measurement included in the probe circuit in order to be used as a magnetic sensor in fusion devices; see section 5.3.
- The Hall voltage provided by sensor BiM5C6 is a lineal function of current supply I_H, where its slope decreases with increasing temperature (see Fig.5.8); see section 5.4.1.
- The Hall voltage provided by sensor BiM4C1 is a non-linear function of magnetic field (see Fig.5.12). The data can be well fitted by equation in the form: $V_H = aB + b \cdot atan(cB)$ and $V_H = a_0 B + b_0 B^2$ (see Fig. 5.13); see section 5.4.2.

- Offset-cancellation electronics was successfully used for measurement of the Hall voltage of sensor BiM4C1(see Fig.5.15a). Its output-to-input voltage ratio is 1145:1; see section 5.5.

Bibliography

[1] M Argüeso, G Robles, and J Sanz. Measurement of high frequency currents with a rogowski coil. *Rev. Sci. Instrum*, 76(6):065107–1, 2005.

[2] Alberto Bilotti, Gerardo Monreal, and Ravi Vig. Monolithic magnetic hall sensor using dynamic quadrature offset cancellation. *IEEE journal of solid-state circuits*, 32(6):829–836, 1997.

[3] I Bolshakova, I Duran, R Holyaka, E Hristoforou, and A Marusenkov. Performance of hall sensor-based devices for magnetic field diagnosis at fusion reactors. *Sensor Letters*, 5(1):283–288, 2007.

[4] Inessa Bolshakova, S Belyaev, M Bulavin, V Brudnyi, V Chekanov, V Coccorese, I Duran, S Gerasimov, R Holyaka, N Kargin, et al. Experimental evaluation of stable long term operation of semiconductor magnetic sensors at iter relevant environment. *Nuclear Fusion*, 55(8):083006, 2015.

[5] F.F. Chen. *Introduction to Plasma Physics and Controlled Fusion: Volume 1: Plasma Physics*. Springer US, 2013.

[6] SN Dange, Ritwik Saha, AM Patade, Ajit Mahadkar, Deepa T Pujara, SV Vansutre, and S Radha. Magnetoresistance of bismuth in bulk and thin film forms. In *SOLID STATE PHYSICS: Proceedings of the 58th DAE Solid State Physics Symposium 2013*, volume 1591, pages 1400–1402. AIP Publishing, 2014.

[7] I Ďuran, S. Entler, M. Kohout, M. Kočan, and G Vayakis. High magnetic field test of bismuth hall sensors for iter steady state magnetic diagnostic.

[8] I Ďuran, J Sentkerestiová, K Kovařík, and L Viererbl. Prospects of steady state magnetic diagnostic of fusion reactors based on metallic hall sensors. In *FUSION FOR NEUTRONS AND SUBCRITICAL NUCLEAR FISSION: Proceedings of the International Conference*, volume 1442, pages 317–324. AIP Publishing, 2012.

[9] I Ďuran, L Viererbl, V Klupák, I Bolshakova, and R Holyaka. Investigation of stability of iter candidate hall sensors under neutron irradiation. *Czechoslovak Journal of Physics*, 56(2):B54–B60, 2006.

[10] Ivan Ďuran, Olena Hronová, Jan Stöckel, Jana Sentkerestiová, and Josef Havlicek. Magnetic measurements using array of integrated hall sensors on the castor tokamaka). *Review of Scientific Instruments*, 79(10):10F123, 2008.

[11] Ivan Ďuran, Jana Sentkerestiová, Michal Kohout, Radek Mušálek, Ladislav Viererbl, and Karel Kovařík. Recent results and challenges in development of metallic hall sensors for fusion reactors. In *FUSION REACTOR DIAGNOSTICS: Proceedings of the International Conference*, volume 1612, pages 31–34. AIP Publishing, 2014.

[12] I Durana, M Hrona, J Stöckela, L Viererblb, R Všolákb, V Červab, I Bolshakovac, R Holyakac, and G Vayakisd. Stability of the hall sensors performance under neutron irradiation. In *Proc. 12th Int. Congress Plasma Physics*, 2004.

[13] EUROfusion. URL<https://www.euro-fusion.org/>. [cit. 2016-02-05].

[14] Jeffrey P Freidberg. *Plasma physics and fusion energy.* Cambridge university press, 2008.

[15] Jodie Corbridge Gillespie. Measurement of the temperature dependence of radiation induced conductivity in polymeric dielectrics. 2013.

[16] A.A. Harms, K.F. Schoepf, G.H. Miley, and D.R. Kingdon. *Principles of Fusion Energy: An Introduction to Fusion Energy for Students of Science and Engineering.* World Scientific, 2000.

[17] Ian H. Hutchinson. *Principles of plasma diagnostics.* Cambridge university press, 2005.

[18] K. Kovarik, I. Duran, J. Sentkerestiova, and D. Sestak. Test-bench for characterization of steady state magnetic sensors parameters in wide temperature range. *Fusion Eng. Des.*, 88(6-8):1319–1322, 2013.

[19] Martin Libra, Jan Mlynar, and Vladislav Poulek. *Jaderna energie.* ILSA, 2012.

[20] Olof Lindberg. Hall effect. *Proceedings of the IRE*, 40(11):1414–1419, 1952.

[21] Robert MacHenry et al. *The new encyclopaedia Britannica.* Encyclopaedia Britannica (UK) Ltd, 1993.

[22] Institute of Plasma Physics of the CAS. History of the castor tokamak. URL<http://www.ipp.cas.cz>. [cit. 2015-12-11].

[23] FP Orsitto, R Villari, F Moro, TN Todd, S Lilley, I Jenkins, R Felton, W Biel, A Silva, M Scholz, et al. Diagnostics and control for the steady state and pulsed tokamak demo. *Nuclear fusion*, 56(2):026009, 2016.

[24] Radivoje S Popovic. *Hall effect devices.* CRC Press, 2003.

[25] Princeton. The physics of fusion in stars. URL<http://www.astro.princeton.edu/ gk/A403/fusion.pdf>. [cit. 2015-06-12].

[26] John D Ramboz. Machinable rogowski coil, design and calibration. In *Instrumentation and Measurement Technology Conference, 1995. IMTC/95. Proceedings. Integrating Intelligent Instrumentation and Control., IEEE*, page 329. IEEE, 1995.

[27] Jan Scheffel and Per Brunsell. *Fusion Physics: Introduction to the physics behind fusion energy.* Alfven Laboratory KTH, Stockholm, 2007.

[28] J Sentkerestiová, I Ďuran, E Dufková, and V Weinzettl. Comparative measurements of plasma position using coils, hall probes, and bolometers on castor tokamak. *Czechoslovak Journal of Physics*, 56(2):B138–B144, 2006.

[29] Jana Sentkerestiová. Development of hall sensors for steady state magnetic diagnostic of fusion reactors. 2014.

[30] LL Snead, DP White, and SJ Zinkle. Investigation of radiation induced electrical degradation in alumina under iter-relevant conditions. *Journal of nuclear materials*, 226(1):58–66, 1995.

[31] BB Srivastava. Fundamentals of nuclear physics, 2006.

[32] EJ Strait, ED Fredrickson, J-M Moret, and M Takechi. Magnetic diagnostics. *Fusion Science and technology*, 53(2):304–334, 2008.

[33] J-Ch Sublet, James W Eastwood, and J Guy Morgan. The fispact-ii user manual. *CCFE-R*, 11(11), 2012.

[34] R Van Nieuwenhove and L Vermeeren. Study of the radiation induced electromotive force effect on mineral insulated cables for magnetic diagnostics in iter. *Fusion engineering and design*, 66:821–825, 2003.

[35] J Wesson. *Tokamaks Third edition*. Clarendon Press, Oxford, 1987.

[36] Wikipedia. Faraday effect. URL<https://en.wikipedia.org/wiki/FaradayEffect>. [cit. 2015-12-11].